Tumor cell endogenous HIF-1 activity induces aberrant angiogenesis and interacts with TRAF6 pathway required for colorectal cancer development

Glaus Garzon, Jesus F ; Pastrello, Chiara ; Jurisica, Igor ; Hottiger, Michael O ; Wenger, Roland H ; Borsig, Lubor

Abstract: Hypoxia and inflammation are key factors for colorectal cancer tumorigenesis. The colonic epithelium belongs to the tissues with the lowest partial pressure of oxygen in the body, and chronic inflammation is associated with an increased chance to develop colon cancer. How the colonic epithelium responds to hypoxia and inflammation during tumorigenesis remains to be elucidated. Here we show, that murine colon adenocarcinoma cells with attenuated response to hypoxia, due to a knock-down (KD) of HIF-1 , produce smaller and less hypoxic tumors in an orthotopic mouse model when compared to tumors induced with control cells. HIF-1 - KD tumors showed more functional perfused vasculature associated with increased levels of vessel-stabilizing factors and reduced levels of proangiogenic factors, including extracellular matrix protein Cyr61/CCN1. Intratumoral injection of Cyr61 in HIF-1 - KD tumors revealed an in increased vessel permeability and tumor hypoxia. Further bioinformatics analysis identified a possible interaction between HIF-1 and TRAF6, an upstream effector of the NF- B pathway that was confirmed by coimmunoprecipitation in MC-38 and CT26 colon adenocarcinoma cells and in situ by proximity ligation assay. Down-regulation of TRAF6 resulted in virtual abrogation of orthotopic tumor growth. Subcutaneous TRAF6-KD tumors were smaller and contained reduced vessel size and differently polarized macrophages. These data demonstrate that the tumor cell response to increased hypoxia in the colon leads to promotion of nonfunctional angiogenesis, regulated by both hypoxia and TRAF6 pathways.

DOI: https://doi.org/10.1016/j.neo.2020.10.006

NEOPLASIA
www.neoplasia.com
Volume 22 Number 12 December 2020 pp. 745–758

Original Research

Tumor cell endogenous HIF-1α activity induces aberrant angiogenesis and interacts with TRAF6 pathway required for colorectal cancer development ☆, ☆☆

Jesus F. Glaus Garzon [a]; Chiara Pastrello [b]; Igor Jurisica [b,c]; Michael O. Hottiger [d]; Roland H. Wenger [a]; Lubor Borsig [a,e,*]

[a] Institute of Physiology, University of Zurich, Zurich, Switzerland
[b] Krembil Research Institute, UHN, Toronto, ON, Canada
[c] Departments of Medical Biophysics and Computer Science, University of Toronto, Toronto, ON, Canada
[d] Department of Molecular Mechanism of Disease, University of Zurich, Zurich, Switzerland
[e] Comprehensive Cancer Center Zurich, Zurich, Switzerland

Abstract

Hypoxia and inflammation are key factors for colorectal cancer tumorigenesis. The colonic epithelium belongs to the tissues with the lowest partial pressure of oxygen in the body, and chronic inflammation is associated with an increased chance to develop colon cancer. How the colonic epithelium responds to hypoxia and inflammation during tumorigenesis remains to be elucidated. Here we show, that murine colon adenocarcinoma cells with attenuated response to hypoxia, due to a knock-down (KD) of HIF-1α, produce smaller and less hypoxic tumors in an orthotopic mouse model when compared to tumors induced with control cells. HIF-1α-KD tumors showed more functional perfused vasculature associated with increased levels of vessel-stabilizing factors and reduced levels of proangiogenic factors, including extracellular matrix protein Cyr61/CCN1. Intratumoral injection of Cyr61 in HIF-1α-KD tumors revealed an in increased vessel permeability and tumor hypoxia. Further bioinformatics analysis identified a possible interaction between HIF-1α and TRAF6, an upstream effector of the NF-κB pathway that was confirmed by coimmunoprecipitation in MC-38 and CT26 colon adenocarcinoma cells and in situ by proximity ligation assay. Down-regulation of TRAF6 resulted in virtual abrogation of orthotopic tumor growth. Subcutaneous TRAF6-KD tumors were smaller and contained reduced vessel size and differently polarized macrophages. These data demonstrate that the tumor cell response to increased hypoxia in the colon leads to promotion of nonfunctional angiogenesis, regulated by both hypoxia and TRAF6 pathways.

Neoplasia (2020) 22, 745–758

Keywords: Colorectal cancer, Tumorigenesis, Tumor hypoxia, HIF-1α, Inflammation, TRAF6

Introduction

Colorectal cancer is the second and third most frequently occurring cancer in women and men, respectively [1]. Hypoxia and inflammation promote tumorigenesis and metastasis through modulation of the tumor microenvironment. Tumor-promoting inflammation contributes to stromal cell polarization supporting angiogenesis [2]. During tumorigenesis, vessels are frequently structurally and functionally abnormal and leaky, which results in reduced perfusion that contributes to enlargement of hypoxic regions, which promote metastasis but also render tumors resistant to chemo- and radiotherapy [3].

Hypoxia-inducible factor (HIF) is the main regulator of the hypoxic response of tumor cells. HIF is a heterodimer constituted by either HIF-1α or HIF-2α and a common HIF-1β subunit. Under normoxia, the HIF-α subunits are modified by prolyl hydroxylases and destined for proteosomal degradation. Under hypoxia, HIF-α subunits are rapidly stabilized and

* Corresponding author.
E-mail address: lborsig@access.uzh.ch (L. Borsig).
☆ Declaration of Competing Interest: The authors declare that they have no known competing financial interests or personal relationships that could have appeared to influence the work reported in this paper.
☆☆ Funding support: This work was supported by the KFSP *Tumor Oxygenation* of the University of Zurich and by SNF grant PDFMP3_127315 (to R.H.W., M.O.H and L.B.). This work was also supported by the SNF grant #310030-152901 (L.B.). Computational analysis was in part supported by Ontario Research Fund (RDI-34876, GL2-01-030), Natural Sciences Research Council (NSERC #203475), Canada Foundation for Innovation (CFI #29272, #225404, #33536) and IBM.
Received 20 July 2020; received in revised form 4 October 2020; accepted 4 October 2020

https://doi.org/10.1016/j.neo.2020.10.006

translocate to the nucleus, where upon heterodimerization bind to hypoxia response elements, leading to enhance transcription of several hundred target genes [4,5]. Hypoxia and other factors associated with pathological stress, such as inflammation or cancer, trigger HIF expression, stabilization, and activity in immune cells [6]. Tumor cells also directly react to hypoxia through HIF-driven responses and modulate tumor microenvironment, angiogenesis, and inflammation; thereby promoting tumorigenesis. For instance, HIF-1α expression in glioblastoma tumors is responsible for upregulation of chemokines, e.g., CXCL12 that drives bone marrow-derived myeloid cell recruitment, contributing to vascular remodeling [7]. In breast cancer cells, HIF-1α stabilization induces the expression of the extracellular matrix remodeling enzymes lysyl oxidase and MMPs, leading to a more aggressive phenotype and metastasis [8]. However, in colon cancer HIF-1α and HIF-2α apparently have different roles, regulating cell proliferation and anchor-independent growth, respectively [9]. While, the epithelial disruption of HIF-2α significantly decreased neutrophil infiltration in colon cancer [10], HIF-1α stabilization in proximal colon augments inflammation and cancer progression [11].

Chronic inflammatory diseases, including inflammatory bowel disease and Crohn's disease, increase the probability of developing colorectal cancer [12]. Infiltration of immune cells, such as granulocytes, results in increased production of reactive oxygen species that induces genomic instability and results in malignant transformation and inflammatory activation of epithelial cells [13]. The nuclear factor NF-κB is the central transcription factor activated by a variety of inflammatory factors derived from either tumor cells or a tumor microenvironment during malignant progression [14]. The expression of tumor promoting cytokines, such as IL-6 or TNF-α, and antiapoptosis survival genes are dependent on NF-κB, thus making it a critical factor in cancer progression [14,15]. Altered NF-κB activation has been detected in many solid tumors where it regulates the expression of genes affecting proliferation, migration, and apoptosis [14,16]. Tumor initiation in colorectal cancer is dependent on an intact IKKβ-mediated NF-κB signaling [17]. However, the impact of upstream NF-κB mediators such as IKK in colon cancer remains to be defined.

Microbial oxygen consumption and large oxygen diffusion distances lead to an anoxic environment in the lumen of the colon [18]. Therefore, hypoxia is likely a main modulator of cancer progression in the colon epithelium, which together with the omnipresent inflammatory stimuli derived from microbiota promotes tumor inflammation. Previously, we have shown that MC-38 cells express only the HIF-1α subunit, which is the sole driver of hypoxic responses in this cell line [19]. Here we tested the role of HIF-1α in tumor cells on colorectal tumor development in an orthotopic mouse model using MC-38 mouse adenocarcinoma cells, where the stromal compartment has normal HIF-1α activity. Bioinformatics approaches identified a direct interaction between hypoxic and inflammatory signaling pathways required for tumor progression.

Materials and methods

Cell culture

Mouse colon adenocarcinoma cells expressing GFP (MC-38GFP) and CT26 cells were cultured in high glucose DMEM (Sigma) supplemented with 10%FBS, NEAA and 1 mmol/L Na-pyruvate (all Gibco). Cells exposed to hypoxia were grown in a gas-controlled workstation ($InvivO_2$ 400, Baker-Ruskinn Technologies). MC-38-HIF-1α-KD cells were prepared as previously described [19]. MC-38-TRAF6-KD was prepared by lentiviral transduction of shRNA vectors in pLKO.1-puro plasmid (Sigma). shRNA constructs targeting mouse TRAF6 and nontarget controls (Mock) were purchased from Sigma.

Mice

All animal experiments were performed according to the guidelines of the Swiss Animal Protection Law and approved by the Veterinary Office of the Kanton Zurich. C57BL/6 J mice were purchased from Charles River, Germany.

Mouse tumor models

Orthotopic colon tumor model: mice were anesthetized by intraperitoneal injection of ketamine/xylaxine/acepromazine (65/10/2 mg/kg per mouse) in saline buffer. After shaving of the abdominal part, a small incision (2–3 mm) was performed and the cecum was exposed. Using a 27 G needle, 40,000 tumor cells in growth factor-reduced Matrigel (Corning) were injected in the cecum wall and both peritoneal and skin layers were subsequently stitched. For analgesia, mice were subcutaneously injected with Meloxicam, 5 mg/kg (Boehringer Ingelheim) 30 min prior- and 6 h and 24 h postsurgery. Subcutaneous tumor model: mice were injected in the right flank with 500,000 MC-38GFP Mock or TRAF6-KD cells. Tumor size was measured with caliper every day and mice were sacrificed at day 19 after injection or when the tumor volume reached 1 cm^3.

Flow cytometry analysis of tumors

Mice were perfused with phosphate buffer saline (PBS) through the left ventricle and dissected orthotopic tumors were digested with collagenase IV, hyaluronidase and DNAse I (all Sigma) in 2% fetal bovine serum/RPMI (FBS/RPMI) for 1 h at 37 °C. The cell suspension was filtered through a 100-μm cell strainer, erythrocytes lysed, and filtered through a 40-μm cell strainer (BD). Cells were stained with Zombie Fixable Viability Kit (Biolegend) and incubated with anti-CD16/32 for 10 min in FACS buffer (PBS/10 mmol/L EDTA, 2% FCS), followed by incubation with antibodies: anti-CD45 (clone 30-F11), anti-CD11b (clone M1/70), anti-Ly6G (clone 1A8), anti-Ly6C (clone HK1.4); all from Biolegend. In case of subcutaneous tumors the following antibodies were used in addition: anti-CD11c (clone N418), anti-CD64 (clone X54–5/7.1), anti-CD103 (clone 2E7), anti-MHCII (clone M5/114.15.2), anti-CD206 (clone C068C2) and anti-VCAM1 (clone 429); all from Biolegend. Data were acquired with a LSR II Fortessa cytometer (BD) and analyzed by FlowJo software v. 7.6.5 (TreeStar).

Hypoxia staining and angiogenic analysis of tumors

Mice were i.v. injected with 1.5 mg pimonidazole (Hypoxyprobe) one hour before termination. For determination of tissue perfusion, mice were i.v. injected with 100 μg FITC-labeled *Lycopersicon esculentum* (tomato) lectin (Vector Labs) 5 min prior to whole body perfusion with PBS followed by tumor dissection and embedding in OCT (TissueTek). Tissue sections (5 μm) were fixed for 10 min in ice-cold acetone, rehydrated in PBS and blocked with 1%BSA in PBST (PBS/0.1% Tween 20) for one hour at room temperature (RT). Sections were then incubated with anti-pimonidazole (Omni Kit Hypoxyprobe) and anti-CD31 (Biolegend) antibodies overnight at 4 °C in blocking buffer. After washing with PBST (3×), antibodies: anti-rabbit-AF568, anti-rat-AF647 (Life Technologies) were incubated for 1 h at RT, counterstained with DAPI (Sigma) and mounted in Prolong Gold (Life Technologies). Pericytes were stained with anti-NG2 (Millipore). Pimonidazole, CD31 or NG2 staining was determined using MIRAX MIDI Slide Scanner (Zeiss). Images were acquired with a CLSM SP5 Resonant APD Confocal Microscope (Leica) and analyzed with the Imaris software (Bitplane). Vessel area was calculated using the software Pannoramic Viewer 1.15.2 (3D Histech).

Vascular permeability assay

Mice with orthotopic tumors were intratumorally injected with recombinant Cyr61 (400 ng, Cusabio Biotech) reconstituted in HBSS every other day starting on day 21 after tumor cell injection (3× in total). Prior to termination, mice were injected with pimonidazole (as described above) followed by i.v. injection of Evans Blue (2 mg) and terminated 30 min later; dissected tumors were embedded in OCT. Staining of pimonidazole and CD31 was performed as described above. Evans Blue staining was analyzed using optimal excitation and emission filters at 620 and 680 nm, respectively.

Cytokine analysis

Cytokines and chemokines in tumor lysates were analyzed using ProcartaPlex Mouse Panel 1 (26-plex; eBioscience) using a Bio-Plex System (Biorad) with xMAP Luminex technology. Protein concentration was determined using the BCA assay following the manufacturer's instructions (Thermo Fisher).

Gene expression in sorted cells

Cell suspension (described above) was stained with Zombie Fixable Viability Kit followed by incubation with anti-CD16/32 and staining with anti-CD45 (clone 30-F11) and anti-CD31 (clone 390); all from Biolegend. At least 50,000 tumor cells ($CD45^{neg}$,$CD31^{neg}$,GFP^{+}) were sorted per sample. RNA was extracted using RNeasy Plus Mini Kit (Qiagen) and cDNA was synthesized using Omniscript RT Kit (Qiagen). qPCR was performed with KAPA SYBR FAST quantitative PCR (qPCR) Master Mix (KAPA Biosystems) and analyzed in a CFX96 Touch Real-Time PCR Detection System (Biorad).

RNA library preparation

The quantity and the quality of the isolated RNA was determined with a Qubit (1.0) Fluorometer (Life Technologies) and a Bioanalyzer 2100 (Agilent). The TruSeq Stranded mRNA Sample Prep Kit (Illumina) was used in the next steps. Briefly, total RNA samples (100 ng) were poly-A selected and then reverse-transcribed into double-stranded cDNA with Actinomycin D added during first-strand synthesis. The cDNA samples were fragmented, end-repaired and adenylated before ligation of TruSeq adapters. The adapters contain the index for multiplexing. Fragments containing TruSeq adapters on both ends were selectively enriched with PCR. The quality and quantity of the enriched libraries were validated using Qubit (1.0) Fluorometer and the Bioanalyzer 2100.

Cluster generation and sequencing

The TruSeq SR Cluster Kit v4-cBot-HS (Illumina) was used for cluster generation using 8 pM of pooled normalized libraries on the cBOT. Sequencing were performed on the Illumina HiSeq 4000 single end 125 bp using the TruSeq SBS Kit v4-HS (Illumina).

RNA sequencing data analysis

Bioinformatics analysis of RNA sequencing data was performed with SUSHI software [20]. In detail, the raw reads were quality checked using Fastqc (http://www.bioinformatics.babraham.ac.uk/projects/fastqc/) and FastQ Screen (http://www.bioinformatics.babraham.ac.uk/projects/fastq_screen/). Quality controlled reads (adaptor trimmed, first 5 and last 6 bases hard trimmed, minimum average quality Q10, minimum tail quality Q10, minimum read length 20 nt) were aligned to the reference genome (Ensembl GRCh38, not patched) using STAR aligner [21]. Read alignments were only reported for reads with less than 50 valid alignments. Expression counts were computed using feature Counts in the Bioconductor package Subread [22]. Differential expression was computed using the DESeq2 package [23]. The RNAseq data have been deposited in gene expression omnibus database under the accession number (GSE155104).

Protein-interaction network analysis

Differently expressed genes from MC-38 cells cultivated under hypoxia and normoxia were used for further analyses: mouse I2D ver. 2.3 (http://ophid.utoronto.ca/i2d) was used to identify their interacting partners [24]. Resulting network was annotated, analyzed and visualized using NAViGaTOR 3.013 [25]. Gene Ontology enrichment analysis was performed using clusterProfiler_3.16.0 [26] on mouse genome wide annotation (org.Mm.eg.db 3.11.4). Enrichment was performed on Biological Process – BP and Cellular Component – CC. Top 20 terms from each of the ontology were plotted. Mouse gene symbols were converted to human gene symbols using biomaRt 2.44.0 [27], and 568 mouse gene symbols were converted to 526 human gene symbols. Disease enrichment analysis was performed on the list of human gene symbols with DOSE_3.14.0 [28] using DisGeNet (DGN). Plots were obtained using clusterProfiler. All analyses were performed using R 4.0.0. (https://www.r-project.org/).

Immunoprecipitation

MC-38 Mock, HIF-1α-KD and TRAF6-KD cells were cultured under hypoxia (0.2% O_2) for 8 hours with or without LPS stimulation (1 μg/mL) for 1 h at 37 °C. Cells were resuspended in lysis buffer (10 mM Tris-HCl pH 8.0, 1 mM EDTA, 400 mM NaCl, 0.1% NP-40) and Sigma's Protease Inhibitor Cocktail. Total protein amount was determined using the BCA assay. Total lysate (1.5 mg) was incubated with 6 μg anti-TRAF6 (Clone: D-10, Santa Cruz) or anti-HIF-1α antibody (Clone: H1α67, Santa Cruz) and 40 μL Dynabead Protein G (ThermoFisher) slurry overnight at 4 °C. Beads were washed with PBS (3×), boiled in Laemmli buffer at 95 °C for 5 min. The supernatant was separated by 10% SDS-PAGE, transferred to a nitrocellulose membrane, and incubated with anti-HIF-1α (rabbit polyclonal, Novus Biologicals) or anti-TRAF6 (Clone: EP591Y, Abcam) antibodies, respectively.

Immunohistochemistry

Tissue paraffin sections (5 μm) were stained with hematoxylin/eosin or the following antibodies: Ki67 (NeoMarkers), and cleaved caspase-3 (Cell Signaling). Staining was performed on a NEXES immune-histochemistry robot (Ventana Instruments) using an IVIEW DAB Detection Kit (Ventana Instruments) or on a Bond MAX (Leica). Images were digitized with a Axio Scan.Z1 slide scanner (Zeiss) and analyzed using Zen Blue image analysis software (Zeiss) and Fiji (ImageJ). Tissue sections were stained simultaneously for each antigen and the signal-to-noise cutoff was manually adjusted for each antibody staining and applied to all samples within one staining group.

Proximity ligation assay

MC-38 cells were cultured on coverslips (12 mm diameter) under normoxia (21% O_2) or hypoxia (0.2% O_2) for 8 h. Cells were washed with 1× PBS and fixed with 4% paraformaldehyde (PFA) for 15 min at room temperature. Samples were washed twice with 1× PBS and permeabilized with 0.1% Tween-20 in 1× PBS for 10 min at room temperature. Duolink

In Situ Orange Starter Kit Mouse/Rabbit (Sigma) was used together with a mouse-anti HIF1α (Clone: H1alpha67, Novus Biologicals) and rabbit-anti TRAF6 (ab33915, Abcam) antibodies were used at 20 μg/mL. Blocking and staining was performed following manufacturer's recommendations.

Statistical analysis

Statistical analysis was performed with the GraphPad Prism software (version 6.03). All data are presented as mean ±SEM and were analyzed by ANOVA with the post-hoc Bonferroni multiple comparison test. Analysis of 2 groups was performed with Mann-Whitney test unless stated otherwise.

Results

Impaired hypoxic response in colorectal tumor cells results in smaller orthotopic tumors

To test how impaired responsiveness of tumor cells to hypoxia affects tumorigenesis, we tested the growth of mouse colon carcinoma cells (MC-38) with stable down-regulation of HIF-1α (HIF-1α-KD) in an orthotopic model. We previously showed that the hypoxic response in MC-38 cells is solely dependent on HIF-1α [19]. We confirmed that MC-38 HIF-1α-KD cells have reduced HIF-1α mRNA levels and minimally respond to hypoxia (Supplementary Figure 1). Intracecal injection of HIF-1α-KD cell resulted in reduced tumor growth when compared to control MC-38 (Mock) cells (Figure 1A). Since hypoxia had previously been shown to attenuate inflammatory responses in MC-38 cells in vitro [19], we analyzed the composition of the immune cells in the tumor microenvironment by flow cytometry. Analysis of tumor infiltrating cells revealed a reduced number of granulocytes ($Ly6G^+$ cells), but increased presence of inflammatory monocytes ($Ly6C^+$ cells) in HIF-1α-KD tumors, when compared to Mock tumors (Figure 1B). We observed no major changes in the number of macrophages; $CD64^+CD11c^-$; or tumor-associated macrophages; TAMs - $CD64^+CD11c^+$; (Supplementary Figure 1D-E). Neither there were any significant changes in polarization of macrophages or TAMs. Histological analysis of tumors showed a reduced presence of $Ly6G^+$ cells. However, no changes in numbers of myeloid cells ($CD11b^+Ly6C^-Ly6G^{lo}$) were observed (Figure 1B). To understand the changes in tumor infiltration of innate immune cells caused by reduced HIF-1α activity, we analyzed the levels of cytokines in tumor homogenates (Figure 1C). Increased levels of CCL2 and CCL7 were detected in HIF-1α-KD tumors, which correlated with the enhanced presence of inflammatory monocytes (Figure 1D).

HIF-1α-KD tumors are less hypoxic and contain more functional vessels

To assess whether the reduced hypoxia response in tumor cells alters hypoxia in HIF-1α-KD tumors, we injected pimonidazole, which forms covalent adducts if the oxygen partial pressure falls below approximately 10 mm Hg. Significant reduction of the hypoxic region was detected in HIF-1α-KD tumors when compared to Mock tumors of similar size (Figure 2A). Next, we analyzed the tumor vasculature and determined the size of blood vessels (vessel area) that allows assessment of angiogenesis. We observed larger vessel areas ($CD31^+$) in hypoxic (pimonidazole$^+$) regions when compared to nonhypoxic (pimonidazole$^-$) regions, which was independent of HIF expression by tumor cells (Figure 2B). This observation is in agreement with the well-known effect of hypoxia on induction of vessel formation [29]. However, HIF-1α-KD tumors showed a reduced intra-tumoral total number of vessels when compared to Mock tumors (Figure 2C), indicating changes in angiogenesis. When we analyzed the vessel maturation by detection of pericytes, using anti-NG2 Ab, a significantly increased number of immature, NG2-negative vessels were detected in Mock tumors when compared to HIF-1α-KD tumors (Figure 2C). The vessel functionality was determined with tomato lectin-FITC perfusion of tumor-bearing mice (Figure 2D). HIF-1α-KD tumors showed more perfused, tomato lectin-positive, vessels. The number of perfused vessel was higher in HIF-1α-KD tumors irrespective of hypoxic and nonhypoxic tumor regions. The correlation between the degree of vessel perfusion and the pimonidazole staining confirmed the increased perfusion in HIF-1α-KD tumors (Figure 2E). To determine how the reduced responsiveness of tumor cells to hypoxia affects tumor angiogenesis, we analyzed tumor lysates using an angiogenesis protein antibody array (Supplementary Figure 2). The analysis of 53 different proteins showed higher amounts of proangiogenic factors (e.g., angiopoetin-1, Cyr61) in Mock tumors when compared to HIF-1α-KD tumors. These data indicate that the impaired hypoxia response in HIF-1α-KD colorectal tumors is associated with reduced vessel formation.

Alterations of inflammatory and angiogenic genes in orthotopic HIF-1α-KD tumors

To understand the role of HIF-1α on tumor growth, we sorted MC-38GFP tumor cells from orthotopic HIF-1α-KD and Mock tumors and analyzed the transcriptome using RNA sequencing. In HIF-1α-KD tumor cells we found 280 genes significantly upregulated ($P< 0.05$), while 288 genes were downregulated when compared to Mock tumor cells (Figure 3A, Table S1).

Gene ontology enrichment analysis using clusterProfiler_3.16.0 on mouse genome wide annotation revealed an upregulation of genes involved in biological processes and cellular components (Figure 3B). Specifically, regulation of vasculature development and angiogenesis together with cell chemotaxis were increased in HIF-1α-KD tumor cells when compared to Mock tumor cells. Simultaneously, cellular components of extracellular matrix and basement membrane genes were increased. The disease enrichment analysis of identified genes in DisGeNET (a curated human dataset of gene-disease association [30] confirmed the tumor angiogenesis as one of the significantly upregulated pathways (Supplementary Figure 3)). To understand the observed changes in leukocyte infiltration and angiogenesis, we focused on genes involved in these processes. Several genes involved in angiogenesis and vessel maturation, including endostatin gene *Col18a1, Pdgfa Peli1 Angptl4* and *Cyr61*, were found to be differentially regulated (Figure 3C). Interestingly, factors contributing to blood vessel stabilization, such as endostatin derived from collagen XVIII and *Pdgfa*, were upregulated in HIF-1α-KD tumor cells.

Endostatin production depends on the proteolytic cleavage of collagen XVIII by matrix metalloproteinases [31]. Indeed, higher MMP9 expression was detected in lysates of HIF-1α-KD tumors (Supplementary Figure 2), which is in agreement with observed reduced number of blood vessels (Figure 2C). In addition, factors inducing inflammatory responses, like *Peli1, Pgts2, Socs3,* and *Tnfrsf9*, were downregulated, while an inhibitor of the NF-κB pathway (*Nfkbie*) was upregulated in HIF-1α-KD tumor cells. Validation of several identified mRNA species by real-time qPCR confirmed the downregulation of the proangiogenic *Cyr61*and *Pgts2* as well as the proinflammatory *Cox2 and Tnfrsf9* transcripts and the upregulation of a vessel-stabilizing factor *Pdgfa* in HIF-1α-KD tumor cells (Figure 3D). Of note, expression of carbonic anhydrase 9, a typical marker of hypoxia, was also reduced in HIF-1α-KD tumor cells. These data show that the hypoxic response in tumor cells directly induces the release of factors modulating inflammation and angiogenesis within the tumor microenvironment.

Since HIF-1α expression in colorectal cancer correlates with poor prognosis [32,33], we examined human colorectal tumor samples in the Medisapiens database (http://ist.medisapiens.com/) for the expression of HIF-1α and transcripts identified to be dysregulated in HIF-1α-KD tumor cells. The analysis of 991 patients dataset showed a direct correlation between *HIF-1A* mRNA levels and *LOX, CYR61, PGTS2, SOCS3, TIMP3, PELI1, TNFRSF9,* and *ANGPTL4* (Supplementary

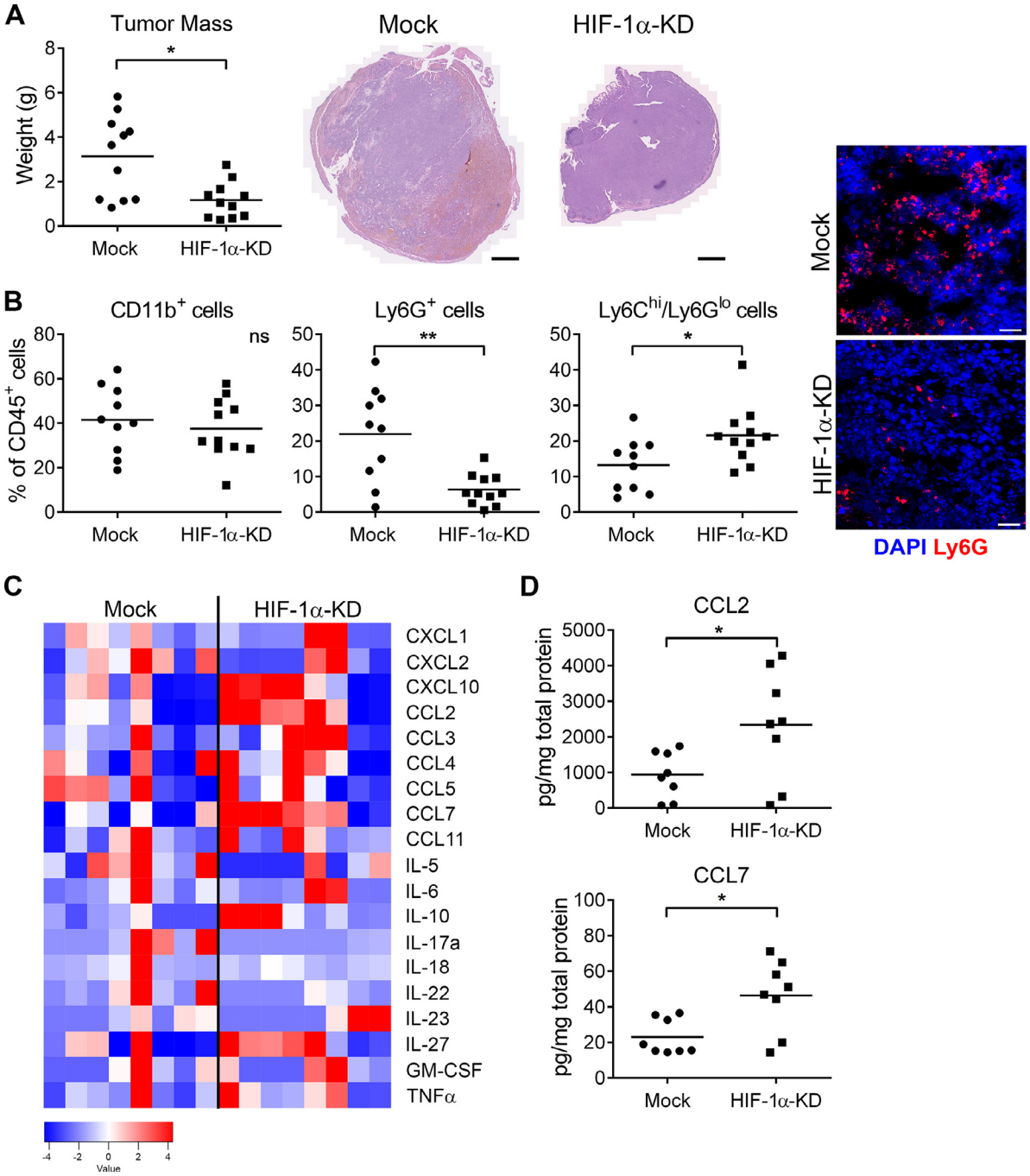

Figure 1. MC-38 colorectal tumor cells with reduced HIF-1α transcript levels lead to reduced orthotopic tumor growth associated with changes in tumor microenvironment. (A) Weight of tumors 28 days after intracecal injection of HIF-1α-KD and control (Mock) MC-38 cells (left panel). Representative images of H&E stained tumors from respective tumors (right panel). Scale bar = 1 mm. (B) Flow cytometry analysis of immune cells in tumors: $CD11b^+/Ly6C^-/Ly6G^{lo}$ myeloid cells (left panel); $Ly6G^+$ granulocytes (middle panel), $Ly6C^{hi}/Ly6G^{lo}$ inflammatory monocytes (right panel) presented as percentage of total living $CD45^+$ cells. Representative images of orthotopic tumors stained with Ly6G-antibody (red) and counterstained with DAPI. Bar = 30 µm. (C) Amounts of cytokines detected in tumor homogenates at day 28. (D) Amounts of Ccl2 and Ccl7 chemokines in tumor homogenates. Statistical significance was assessed using the Mann-Whitney test; *, $P < 0.05$; **, $P < 0.01$. (Color version of figure is available online.)

Figure 4A), which is in agreement with data obtained from the MC-38 mouse model. Similarly, the analysis using 594 colorectal cancer patient samples from Colorectal Adenocarcinoma dataset (TCGA, PanCancer Atlas; https://www.cbioportal.org/ ver. 3.4.3) confirmed the significant correlation between HIF-1α and the genes identified in MC-38 model (Supplementary Figure 4B).

Intratumoral delivery of CYR61 increases tumor hypoxia and vascular permeability in HIF-1α-KD tumors

Pathologic tumor neovascularization and aggressiveness have been linked to the expression of Cyr61/CCN1 in breast and pancreatic cancer cells [34–36]. Cyr61 is an extracellular matrix protein promoting

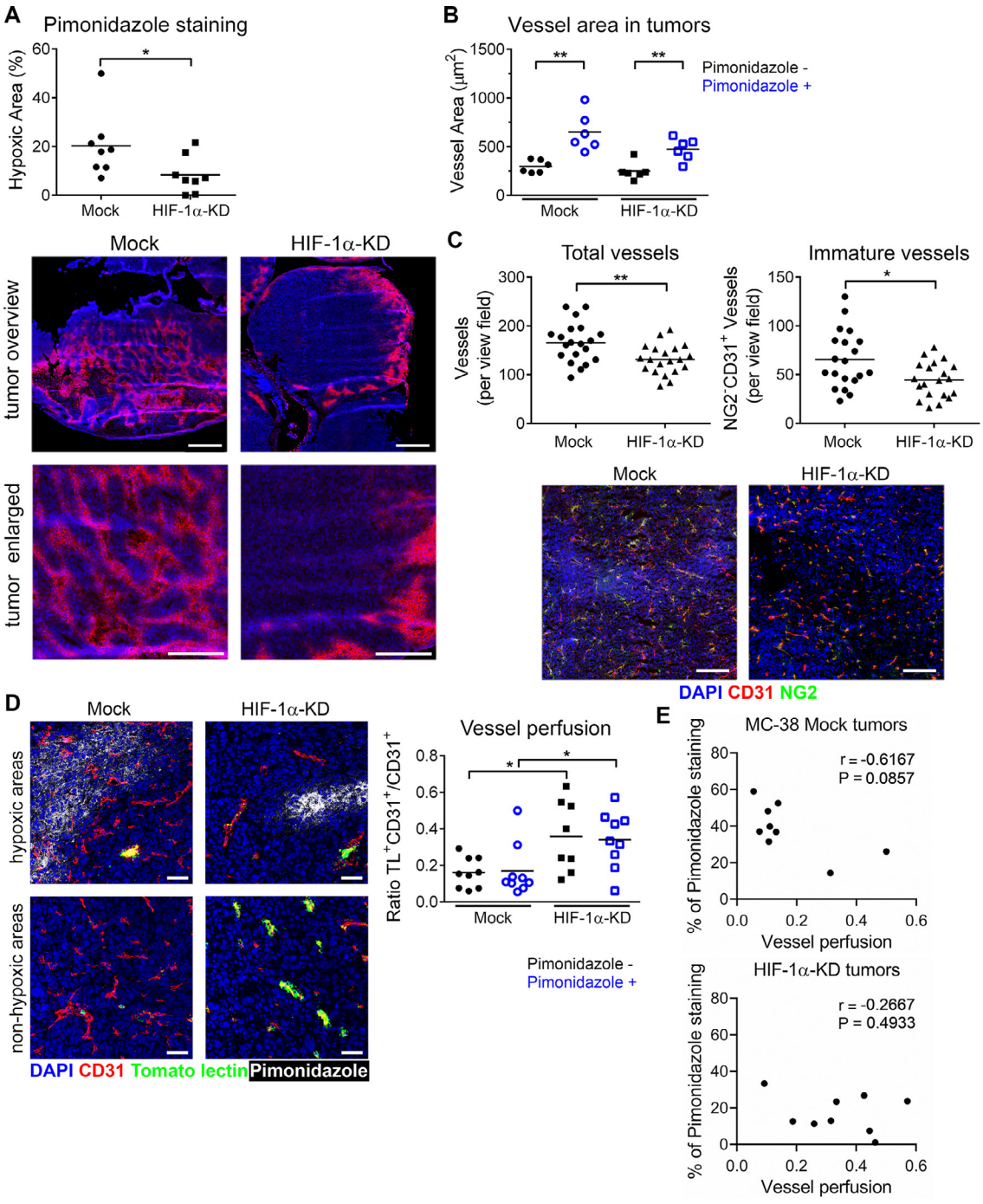

Figure 2. Impaired HIF-1α signaling in MC-38 tumor cells results in vascular normalization in tumors. (A) Quantification of hypoxic regions in tumors as percentage of pimonidazole positive area over total tumor area in Mock and HIF-1α-KD tumors. Representative images of hypoxic regions in cecum tumors visualized by pimonidazole staining, red; counterstained with DAPI, blue (lower panel). Scale bar = 1 mm (overview); scale bar = 500 μm (enlarged) panels. (B) Total vessel area in pimonidazole positive and negative regions of orthotopic tumors determined by counting of CD31-positive vessels. Comparison of Mock and HIF-1α-KD tumors from 3 independent experiments. (C) Total number of vessels ($CD31^+$) per view field (PVF) in Mock and HIF-1α-KD tumors (left panel) and immature vessels as determined by NG2-staining of pericytes; $NG2^-CD31^+$; (right panel). Representative immunofluorescence images of tumors stained for NG2 (green), CD31 (red) and DAPI (blue). Three random view fields were counted per tumor, $n = 4$–5 mice per group. Scale bar = 200 μm. (D) Representative images of vessels perfused with tomato lectin (TL; green) in pimonidazole positive (white) and pimonidazole negative tumors regions. Vessels were stained with CD31 Ab (red) and counter-stained with DAPI (blue). Scale bar = 50 μm. Ratio of perfused vessels ($TL^+/CD31^+$) over total number of vessels ($CD31^+$) per view field, assessed in both pimonidazole positive and negative regions (right panel). Three random view fields were analyzed per tumor, $n = 3$ per mouse group. Mice from 3 independent experiments were analyzed at day 28 post-tumor cell injection in panels A-C. (E) Correlation analysis between the degree of tumor perfusion and tumor hypoxia (pimonidazole-positive areas) in Mock and HIF-1α-KD tumors, respectively from histological sections shown in panel D. Statistical significance was assessed using the Mann-Whitney test; *, $P < 0.05$; **, $P < 0.01$. (Color version of figure is available online.)

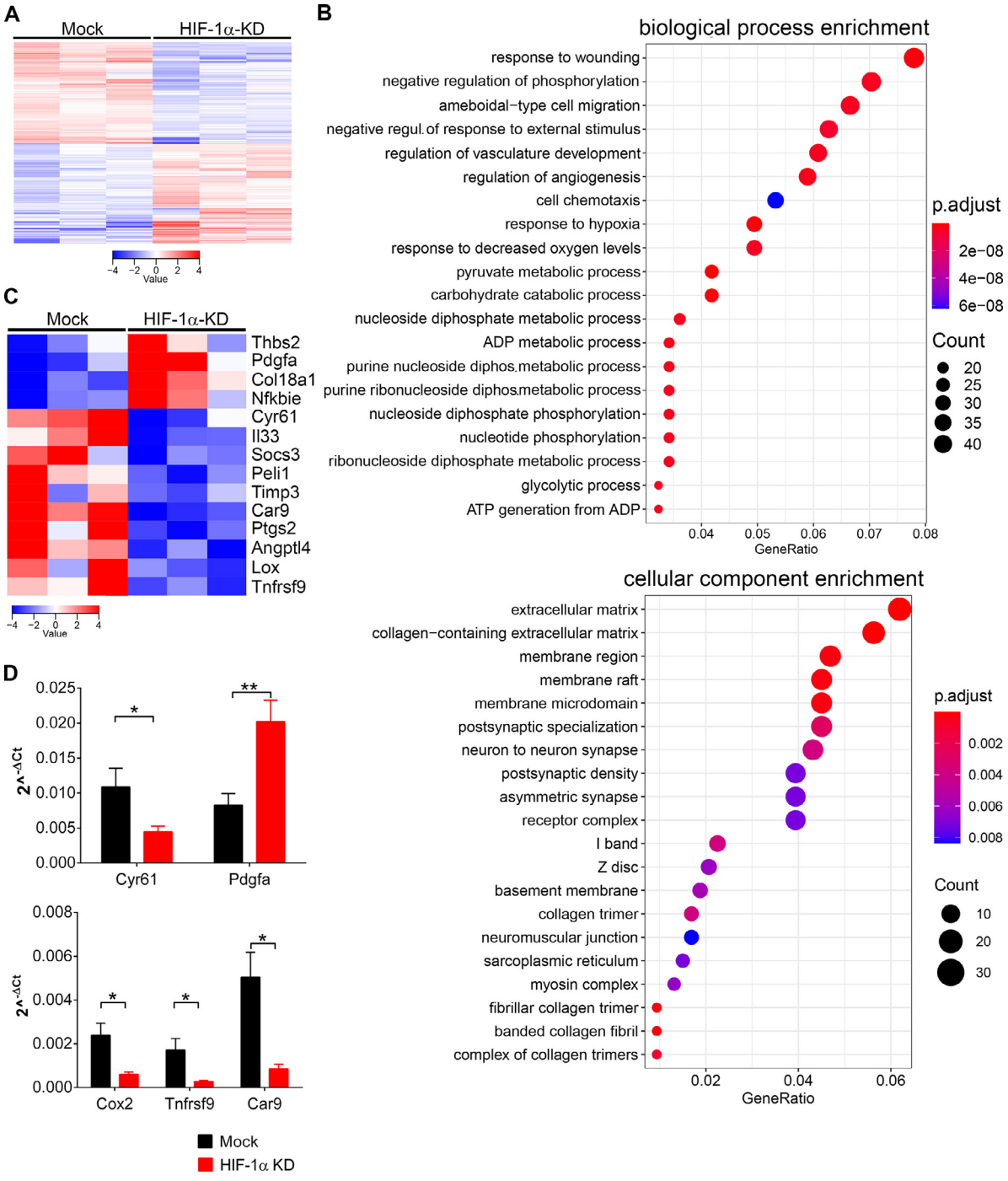

Figure 3. Upregulation of vessel-stabilizing factors and downregulation of proangiogenic molecules in HIF-1α-KD orthotopic tumors. (A) RNA sequencing results from Mock and HIF-KD sorted tumor cells from orthotopic tumors (>50,000 cells) presented as a heatmap. (B) Gene Ontology enrichment analysis performed on genes that were significantly deregulated in sorted HIF-1α-KD when compared to Mock tumor cells. (C) Fourteen genes linked to angiogenesis and inflammation which are differently regulated between HIF-1α-KD and Mock tumor cells. Statistically significant differences: at least $P < 0.01$. (D) Expression levels of selected differentially regulated genes in HIF-1α-KD and Mock tumor cells, normalized to ribosomal protein S12 mRNA, were validated by qPCR ($n = 4–5$). Statistical significance was assessed with Mann-Whitney test; *, $P < 0.05$; **, $P < 0.01$.

endothelial cell proliferation, adhesion, and differentiation [37]. We observed downregulation of Cyr61 in HIF-1α-KD tumor cells (Figure 3C-D) as well as in tumors (Supplementary Figure 2). To test whether Cyr61 affects the tumor growth of colon carcinoma, we intratumorally injected recombinant Cyr61 into HIF-1α-KD tumors. Increased hypoxic regions, determined by pimonidazole staining, were observed upon Cyr61 injection when compared to control tumors treated with the solvent HBSS (Figure 4A). No changes in vessel density were observed between Cyr61 and control tumors in the hypoxic regions while a significant reduction of vessel numbers was observed in pimonidazole-negative regions (Figure 4B). However, Cyr61 injection induced larger vessels, as determined by the vessel area, which correlated with reduced vessel density in pimonidazole-negative regions. To

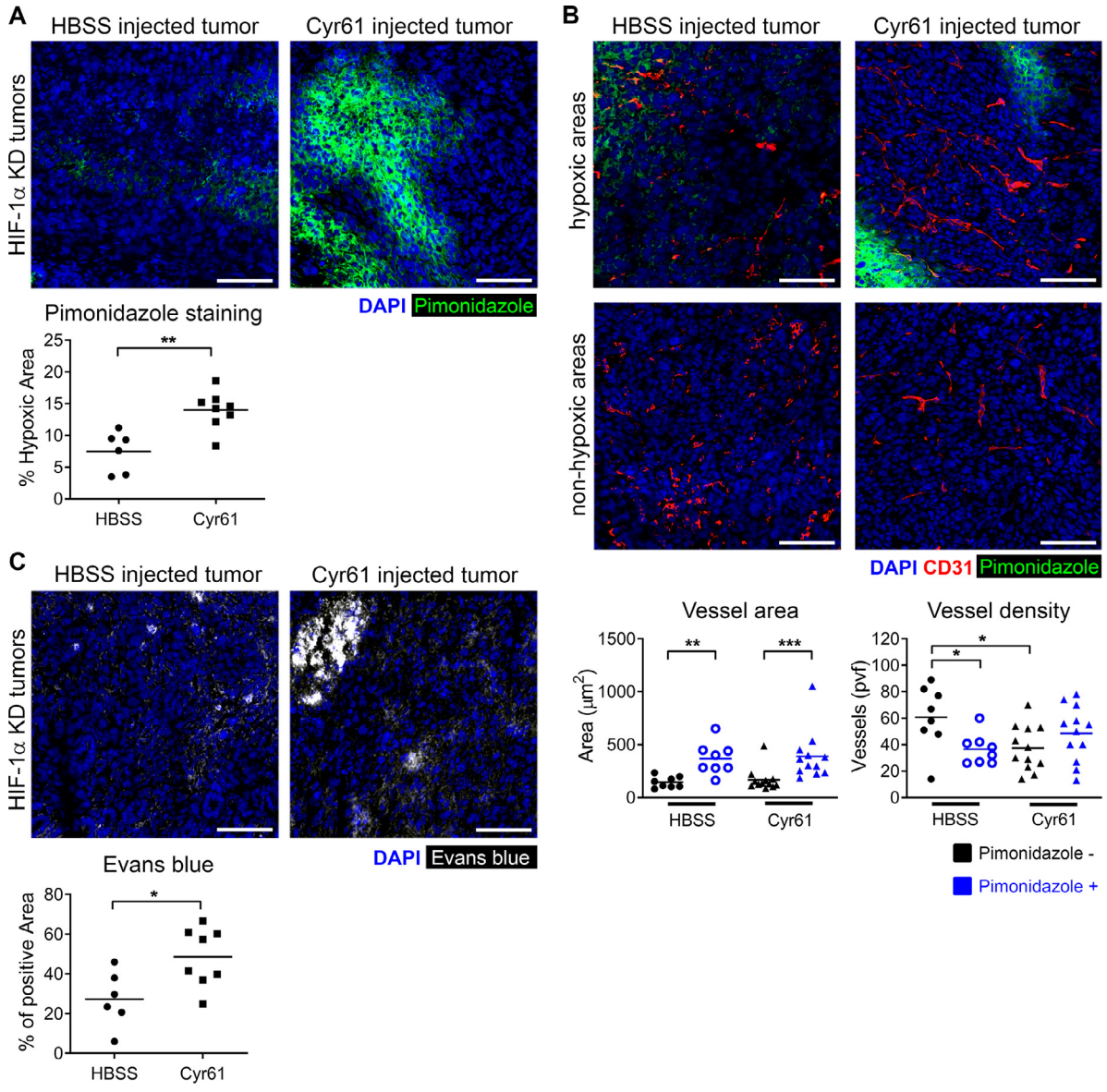

Figure 4. Intratumoral treatment of HIF-1α-KD orthotopic tumors with Cyr61 protein increases tumor hypoxia and vascular leakiness. (A) Representative images of hypoxic regions in HIF-1α-KD tumors treated with Cyr61 or HBSS (control) visualized by pimonidazole staining (green) and counterstained with DAPI (blue). Quantification of hypoxic regions as percentage of pimonidazole positive area over total tumor area in respective tumors (lower panel); n = 6–8 tumors per group. (B) Representative images of blood vessels (CD31 staining, red) in HIF-1α-KD tumors either treated with Cyr61 or HBSS. Hypoxic and non-hypoxic regions visualized by pimonidazole (green) and counterstained with DAPI (blue) for respective treatments. Lower panels show total vessel area ($CD31^+$) and the average vessel density per view field (PVF), determined in randomly chosen 2 view fields per tumor sample ($n = 4–5$ tumors per group). (C) Representative images of Evans Blue staining (white) in HIF-1α-KD tumors treated with either Cyr61 or HBSS. Quantification of vascular permeability in tumors shown as a percentage of Evans Blue positive area over total tumor area ($n = 5–8$ tumors per group). Statistical significance was assessed using the Mann-Whitney test; *, $P < 0.05$; **, $P < 0.01$; ***, $P < 0.001$. (Color version of figure is available online.)

test whether Cyr61 injection affected the functionality of vessels, we injected Evans Blue and assessed extravasation of the dye (Figure 4C). HIF-1α-KD tumors injected with recombinant Cyr61 showed increased vascular permeability, which is in agreement with Cyr61 as an inducer of aberrant tumor angiogenesis associated with nonfunctional leaky vessels and hypoxia.

HIF-1α interacts with TRAF6 upstream of NF-κb in MC-38 cells

Inflammation is directly linked to colon cancer development [12] and the colonic epithelium is known to be in a physiologically hypoxic state [18]. This unique physiological situation in the colon stimulated us to assess the cross talk between inflammation and hypoxia in the mouse colon-cancer model. Previously, we had shown that HIF-1α levels in MC-38 cells remain unchanged upon LPS stimulation, while hypoxia treatment failed to induce NF-κB signaling in vitro [19]. We used this dataset of differently expressed genes from MC-38 cells for an *in silico* analysis based on the known proteome-wide physical protein-protein interactions (Figure 5A). Of note, the HIF target and hypoxic tumor hallmark gene carbonic anhydrase 9 (CA9) was identified among the upregulated genes, which confirms the hypoxic culture conditions. Among the identified sixty proteins, the tumor

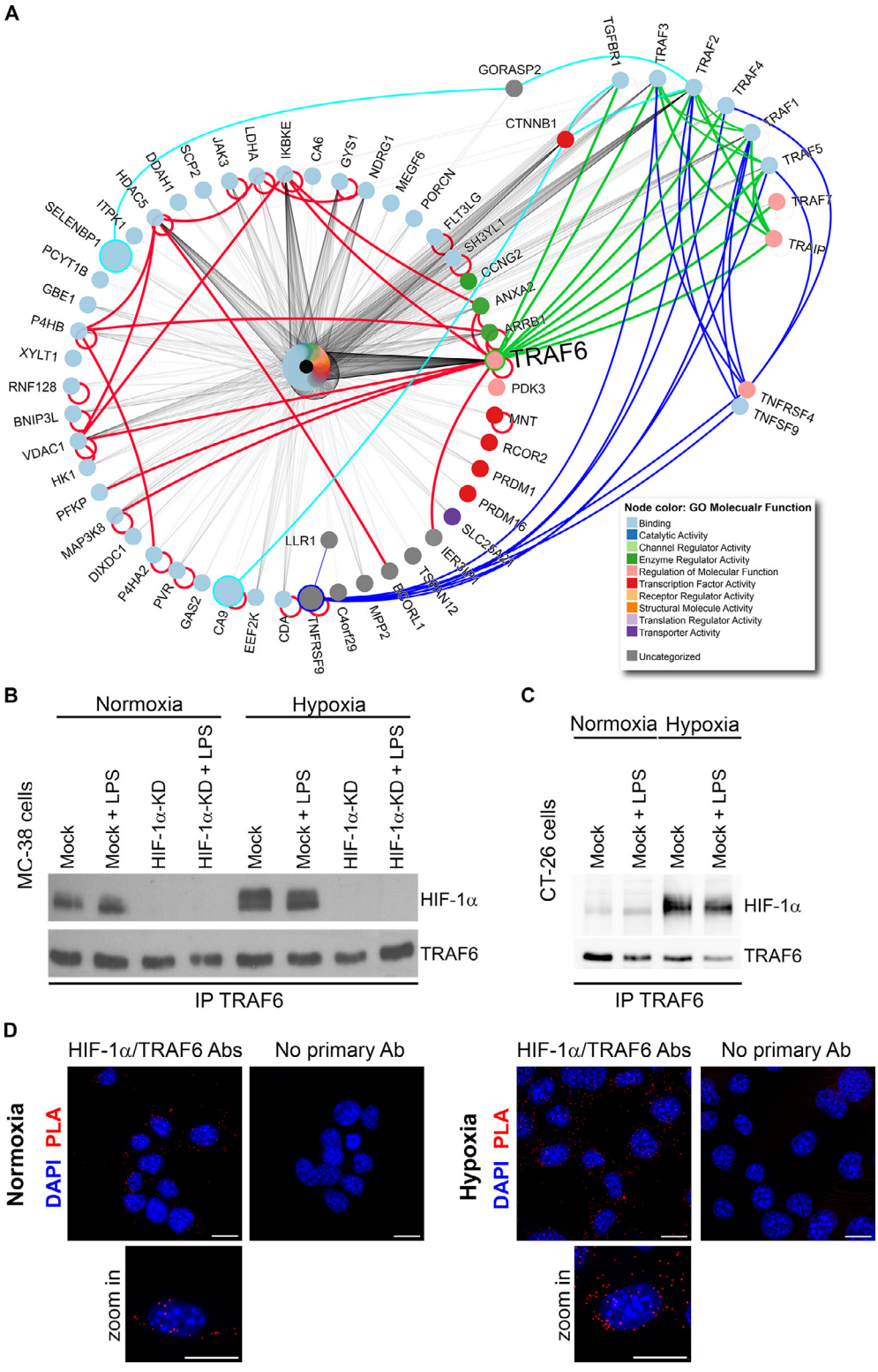

Figure 5. HIF-1α interacts with TRAF6 and links hypoxia to inflammation in colorectal cancer. (A) Protein-protein interaction network based on differently regulated genes observed in MC-38 cells cultured under either hypoxia or normoxia using the NAViGaTOR software. Node size is proportional to the expression level in hypoxia versus normoxia. Red lines represent direct interactions among proteins upregulated during hypoxia. Blue, turquoise, and green lines show indirect/mediated interactions of the TRAF6 with other hypoxia upregulated proteins. (B) Coimmunoprecipitation of TRAF6 and HIF-1α in Mock and HIF-1α-KD MC-38 cells stimulated either by hypoxia/normoxia with or without addition of LPS followed by the detection of TRAF6 or HIF-1α, respectively (n = 3). (C) Co-immunoprecipitation of TRAF6 and HIF-1α in CT26 cells stimulated either by hypoxia/normoxia or LPS addition, followed by the detection of TRAF6 or HIF-1α, ($n = 3$). (D) Proximity ligation assay in MC-38 Mock cells cultured under normoxia and hypoxia for 8 h followed by detection with HIF-1α and TRAF6-specific antibodies using Duolink In Situ Orange Kit (Sigma). Negative control (No primary Ab) is shown; scale bar = 15 µm. (Color version of figure is available online.)

necrosis factor receptor-associated factor 6 (TRAF6) protein was identified as a possible key interaction point with the highest centrality value between the hypoxic and inflammatory pathways (Figure 5A). Previously, TRAF6 overexpression in tumor cells had been shown to stabilize HIF-1α [38]. Thus, we tested the hypothesis that TRAF6 directly interacts with HIF-1α, as suggested from the protein-protein interaction network analysis. HIF-1α-KD and Mock MC-38 cells were cultured under normoxia and hypoxia, with or without LPS stimulation, followed by TRAF-6 immunoprecipitation and HIF-1α detection (Figure 5B). Increased co-immunoprecipitated HIF-1α protein amounts were detected in Mock cells under hypoxia when compared to normoxia, indicating physical interaction between TRAF6 and HIF-1α. When HIF-1α was immunoprecipitated in MC-38 cells stimulated with hypoxia, TRAF6 protein was detected (Supplementary Figure 5). LPS stimulation alone had no effect on HIF-1α expression (Figure 5B), which is in agreement with our previous data [19]. To demonstrate that the HIF-1α-TRAF6 interaction is not cell type specific, coimmunoprecipitation was confirmed in murine CT26 colon carcinoma cells (Figure 5C). Next, we confirmed the TRAF6-HIF-1α interaction using proximity ligation assay in situ. MC-38 Mock cells under normoxia showed interaction between TRAF6 and HIF-1α in the cytoplasm, which was increased in cells cultured under hypoxia (Figure 5D).

TRAF6 is required for orthotopic tumor growth

To test the involvement of TRAF6 in tumorigenesis, we prepared MC-38GFP with shRNA-induced downregulated TRAF6 expression, MC-38-TRAF6-KD (Supplementary Figure 6A-C), and injected them into the cecum wall. Interestingly, only three out of twenty one animals developed a very small tumor upon MC-38-TRAF6-KD tumor cells injection while all Mock cell injections led to tumor formation (Figure 6A). To exclude that TRAF6-KD tumor cells have a general problem to proliferate in vivo, we intravenously injected these cells and followed metastasis to the lungs. Lung tumors grew in all mice injected with MC-38-TRAF6-KD cells at similar size as with Mock cells, albeit in reduced numbers (Supplementary Figure 6D). Subcutaneous injection of MC-38-TRAF6-KD tumor cells also resulted in normal tumor development, albeit the size of tumors was reduced when compared to Mock tumors (Figure 6B). These data indicate that TRAF6 in colorectal tumor cells is essential for tumor growth specifically in the colon/cecum.

Next, we analyzed the composition of TRAF6-KD and Mock subcutaneous tumors. TRAF6-KD tumors showed an increased detection of apoptotic cells, as determined by cleaved-caspase 3 staining, when compared to Mock tumors, which correlates with reduced tumor size (Figure 6C). Interestingly, TRAF6-KD tumor showed also increased number of Ki67-positive tumor cells. No major changes in macrophages between TRAF6-KD and Mock tumors were observed using immunohistochemistry (Figure 6D). Flow cytometry analysis of tumor infiltrating leukocytes revealed an increased presence of inflammatory monocytes ($Ly6C^{hi}$), and reduced numbers of myeloid cells ($CD11b^{+}$) and tumor-associated macrophages; TAMs ($CD11b^{+}CD64^{+}CD11c^{+}$) in TRAF6-KD tumors (Figure 6D). The number of macrophages ($CD64^{+}CD11c^{-}$) remained unchanged between TRAF6-KD and Mock tumors. When we analyzed the polarization of macrophages into protumorigenic M2 or antitumorigenic M1 one using the CD206 and MHCII markers, respectively, increased numbers of M1 type macrophages in TRAF6-KD were observed (Figure 6E), which is in agreement with the observed tumor size reduction (Figure 6B).

TRAF6-KD tumors show reduced vessel density

TRAF6 had previously been shown to modulate HIF-1α expression in colonic and breast cancer tumor cells [38,39], and here we showed that TRAF6 interacts with HIF-1α in murine MC-38 and CT-26 cells. Thus, we asked whether TRAF6-KD affected tumor angiogenesis. While the number of vessels was not affected in TRAF6-KD tumors, a significantly reduced vessel area, reflecting reduced angiogenesis, was observed when compared to Mock tumors (Figure 6F). These results indicate that that functional TRAF6 signaling contributes to formation of aberrant blood vessels in the tumors, reflected in significantly larger vessels.

Discussion

Inflammation and hypoxia modulate the tumor microenvironment to promote tumor progression and invasiveness [40]. Low oxygen tensions, present at both inflammatory sites and tumors, stabilize HIF-αs, which activates target genes involved in angiogenesis, cell survival, metabolic reprogramming, and metastasis. Overexpression of HIF-1α was observed in various human cancers, including colorectal cancer [41] and is independently associated with poor prognosis [32]. HIF-1α is a transcription factor regulating tumor cell survival and proliferation; and epithelial barrier function following inflammation in the colon [11,42,43]. Here we studied the role of HIF-1α-mediated response towards hypoxia in an orthotopic colorectal cancer model in immunocompetent mice. Importantly, we observed smaller HIF-1α-KD tumors, with reduced infiltration by granulocytes. The almost complete absence of a hypoxic response in MC-38 cells resulted in tumors with less but more functionally perfused vasculature. The number and the size of blood vessels in Mock tumors correlated with increased tumor hypoxia indicating an active role of tumor cell-derived HIF-1α signaling leading to aberrant, non-functional angiogenesis [3]. In this context, down-regulation of HIF-1α in tumor cells resulted in vessel normalization and maturation, and consequently less hypoxia. Of note, increased local oxygen consumption by infiltrating granulocytes with active respiratory burst contributes to intestinal tissue hypoxia in colitis models [44]. Indeed, we observed higher numbers of granulocytes in Mock tumors. Recently, metabolic targeting of HIF-1α has been shown to potentiate chemotherapy responses in human colorectal cancer tumor growth in a murine model, which was associated with reduced angiogenesis [45]. These findings are in agreement with our data showing that MC-38 tumors with reduced HIF-1α expression are smaller, with functional vessels and reduced hypoxia. In addition, better-perfused vasculature may explain the increased responsiveness to chemotherapy observed previously [45]. Recent study provided evidence for microRNA regulated switch between endothelial cell proliferation and migration during angiogenesis [46]. Specifically, miRNA-29a-3p was found to be a selective marker identifying colorectal cancer patients, who are responding to anti-angiogenic treatments. Using mirDIP database portal we identified possible hsa-miR-29a-3p target genes in our tumor dataset. Interestingly, 81 targets overlap with upregulated genes and 87 targets with down-regulated genes (Supplementary Figure 7); including upregulated genes involved extracellular matrix modification and downregulated expression of Cyr61. Further studies are required to assess the role of the tumor hypoxia status and its effect on miRNA regulated angiogenesis.

The balance between pro- and anti-angiogenic factors is usually disturbed during tumor development, resulting in tortuous and leaky vessels [47]. Analysis of tumor lysates showed reduced amounts of inflammatory and pro-angiogenic factors in HIF-1α-KD tumors, such as Cyr61 or Dll4, which correlated with a normalized vasculature. Transcriptome analysis of sorted MC-38 tumor cells revealed upregulation of vessel-stabilizing factors such as endostatin, Pdgfa, Thbs2 in HIF-1α-KD cells and reduced expression of pro-angiogenic factors such as Cyr61, Cox-2 and Angptl4 when compared to Mock tumors. Both findings on mRNA and protein levels are in agreement with histological evidence of more functional vessels detected in tumors with an impaired hypoxia response. Of note, HIF-1α down-regulation resulted in lower transcript levels of genes such as *Pellino1, Socs3* and *Tnfrsf9* involved in

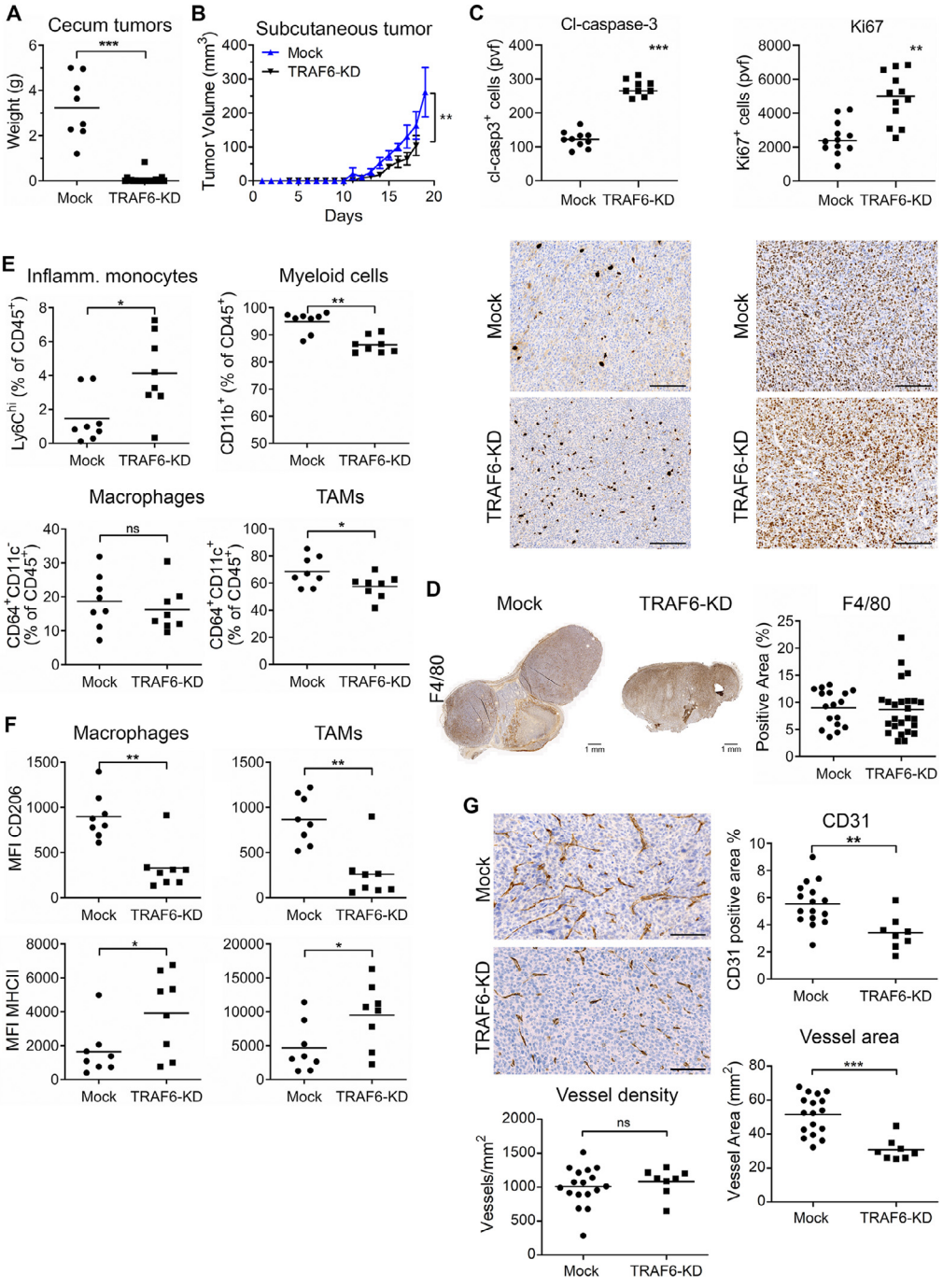

Figure 6. TRAF6-KD in MC-38 cells impairs tumor growth in the cecum and reduced subcutaneous tumor growth with changes in macrophages and angiogenesis. (A) Tumor mass in mice with MC-38 TRAF6-KD and Mock cell injection in the cecum 28 days postinjection. Mice without tumor have zero value. Mice from 2 independent experiments are presented (TRAF6-KD; $n = 21$). (B) The growth of subcutaneous tumors in mice injected either with TRAF6-KD or Mock MC-38 cells (n ≥ 10 per group). (C) Immunohistochemical analysis of cleaved-caspase-3 (cl-casp-3) and Ki67 staining in subcutaneous MC-38 Mock and TRAF6-KD tumors. Random view fields were quantified for positive cells. pvf, per view field; scale bar = 200 μm. (D) Immunohistochemical analysis of subcutaneous tumors stained with the macrophage marker F4/80 Ab (top panels) were quantified (low panel). Three to 4 random view fields were analyzed per tumor; $n = 4$–5 per group. (E) Number of innate immune cells in orthotopic tumors represented as percentage of living $CD45^+$ cells, determined by flow cytometry; inflammatory monocytes, $Ly6C^{hi}$; dendritic cells, $CD103^+/CD64^-$; macrophages, $(CD64^+/CD11c^-/CD103^-$; and tumor-associated macrophages – TAMs, $CD64^+/CD11c^+/CD103^-$. Tumor analysis from two independent experiments ($n = 8$). (F) Cell surface expression of polarization markers MHCII and CD206 was analyzed by flow cytometry, in parallel to the experiments shown under E. MFI from FMO control was subtracted from each sample; MFI, median fluorescence intensity. (G) Angiogenesis in TRAF6-KD and Mock tumors was analyzed using CD31 staining. The amount to vessel (CD31-positive staining) was quantified as percentage of total tumor area; vessel area and vessel density, respectively. Representative images of Mock and TRAF6-KD tumor are shown; scale bar = 100 μm. Statistical significance was assessed using the Mann-Whitney test; *, $P < 0.05$; **, $P < 0.01$; ***, $P < 0.001$.

the inflammatory cascade. In human colorectal tumors, HIF-1α expression positively correlated with genes shown to be regulated by HIF-1α in MC-38 tumors. Particularly, the observed Cyr61 mRNA level was previously reported to be a pro-angiogenic and tumor-promoting factor in renal, breast, pancreas and lung cancer cell lines [48-50]. We showed that intra-tumoral injection of Cyr61 resulted in enhanced angiogenesis associated with increased leaky vasculature and tumor hypoxia. Thus, the interference with the HIF-1α response in tumor cells leads to vessel normalization despite the intact hypoxia response in the tumor microenvironment.

Tumor cell-derived NF-κB signaling is required for tumor initiation and progression in colorectal cancer [17,51]. Specific inactivation of the NF-κB pathway in epithelial cells attenuated the formation of colitis-associated colon cancer [52]. The modulation of NF-κB signaling in colon cancer has been linked to: increased chemokine expression associated with leukocyte infiltration and the microbiota-derived activation [53–55]. Bioinformatics analysis of the potential HIF-1α interactome identified TRAF6, an upstream mediator of the NF-κB pathway, as a potential link between hypoxia signaling and the inflammatory cascade. MC-38 tumor cells with reduced TRAF6 expression could not establish a tumor in the caecum, while tumors readily formed upon subcutaneous injection, albeit at a reduced size. Intestinal epithelial cells are in a constant contact with microbiota, which requires a tight control of inflammatory responses [54,56], likely explaining why tumor cells with reduced TRAF6 activity and therefore reduced NF-κB signaling do not grow in the inflammatory environment of a colon.

The histological analysis of TRAF6-KD tumors showed increased apoptosis (cleaved-caspase-3^{+}), but also increased tumor cell proliferation as determined by Ki67 staining, when compared to Mock tumors. Ki67-staining is routinely being used for detection of proliferating tumors cells in animal models (e.g. [57]. However, recent study showed that Ki67 expression is not always associated with cell proliferation, since the Ki67 gene controls heterochromatin organization [58]. Targeted depletion of Ki67 gene in the mouse gut epithelium did not result in any cell proliferation deficiency. Furthermore, cleaved-caspase 3 detection is a better prognostic marker than Ki67 staining in colorectal and endometrial cancers [59,60]. Recently, suppression of TRAF6 expression through overexpression of miR-146a resulted in deregulation of tumor cell proliferation in non-small cell lung cancer [61]. This finding is in agreement with our observation that TRAF6-KD tumors showed enhanced Ki67 staining, although we observed limited tumor growth due to enhanced apoptosis and reduced angiogenesis.

TRAF6 is a unique member of the TRAF family of intracellular proteins, and is critically involved in the IL-1 receptor and Toll-like receptor family induced signal transduction leading to NF-κB activation [62]. Increased TRAF6 expression has been reported in various tumors, including colon, breast and melanoma cancers, as well as in lymphoid malignancies [38,39,63–65]. Reportedly, TRAF6 is a K63-E3 ubiquitin ligase that ubiquitinates and stabilizes HIF-1α in colon cancer cells independent of oxygen [38]. On contrary to previous findings, we observed enhanced endogenous levels of HIF-1α interacting with TRAF6 under hypoxia. In breast cancer cells, TRAF6 overexpression correlated with increased HIF-1α signaling and metastasis [39]. We identified TRAF6 as a potential binding partner of HIF-1α in MC-38 tumor cells under hypoxia and confirmed that TRAF6 physically interacts with HIF-1α as visualized by proximity ligation assay. Interestingly, we observed mostly cytoplasmic localization of TRAF6-HIF-1α interactions. Our data indicate that TRAF6-HIF-1α interaction contributes to tumor growth, primarily through modulation of angiogenesis, likely through stabilization of HIF-1α proteins levels in tumor cells [38]. Both individual downregulations of either HIF-1α or TRAF6 resulted in smaller tumors with reduced angiogenesis and normalized vasculature. Thus, targeting of hypoxia-inflammatory crosstalk represents an attractive approach for further development of improved delivery of standard or targeted cancer therapies.

Authors' contributions

Conception and design: J.F. Glaus Garzon, R.H. Wenger, M.O. Hottiger, L. Borsig; Development of methodology: J. F. Glaus Garzon, L. Borsig; Acquisition of data/Investigation: J.F. Glaus Garzon; Analysis and validation of data (e.g., statistical analysis, biostatistics, computational analysis): J.F. Glaus Garzon, C. Pastrello, I. Jurisica, L. Borsig; Data curation, visualization: C. Pastrello, I. Jurisica; Resources: M.O. Hottiger, R.H. Wenger, I. Jurisica, L. Borsig; Writing original draft: J.F. Glaus Garzon, L. Borsig; Writing/review/editing of the manuscript: J.F. Glaus Garzon, I. Jurisica, R.H. Wenger, M.O. Hottiger, L. Borsig; Study supervision: L. Borsig.

Supplementary materials

Supplementary material associated with this article can be found, in the online version, at doi:10.1016/j.neo.2020.10.006.

References

[1] Torre LA, Bray F, Siegel RL, Ferlay J, Lortet-Tieulent J, Jemal A. Global cancer statistics, 2012. *CA Cancer J Clin* 2015;**65**:87–108.

[2] Hanahan D, Weinberg RA. Hallmarks of cancer: the next generation. *Cell* 2011;**144**:646–74.

[3] Carmeliet P, Jain RK. Principles and mechanisms of vessel normalization for cancer and other angiogenic diseases. *Nat Rev Drug Discov* 2011;**10**:417–27.

[4] Semenza GL. Oxygen sensing, hypoxia-inducible factors, and disease pathophysiology. *Annu Rev Pathol* 2014;**9**:47–71.

[5] Wenger RH, Stiehl DP, Camenisch G. Integration of oxygen signaling at the consensus HRE. *Sci STKE* 2005;**2005**:re12.

[6] Palazon A, Goldrath AW, Nizet V, Johnson RS. HIF transcription factors, inflammation, and immunity. *Immunity* 2014;**41**:518–28.

[7] Du R, Lu KV, Petritsch C, Liu P, Ganss R, Passegue E, Song H, Vandenberg S, Johnson RS, Werb Z, et al. HIF1alpha induces the recruitment of bone marrow-derived vascular modulatory cells to regulate tumor angiogenesis and invasion. *Cancer Cell* 2008;**13**:206–20.

[8] Cox TR, Rumney RM, Schoof EM, Perryman L, Hoye AM, Agrawal A, Bird D, Latif NA, Forrest H, Evans HR, et al. The hypoxic cancer secretome induces pre-metastatic bone lesions through lysyl oxidase. *Nature* 2015;**522**:106–10.

[9] Imamura T, Kikuchi H, Herraiz MT, Park DY, Mizukami Y, Mino-Kenduson M, Lynch MP, Rueda BR, Benita Y, Xavier RJ, et al. HIF-1alpha and HIF-2alpha have divergent roles in colon cancer. *Int J Cancer* 2009;**124**:763–71.

[10] Triner D, Xue X, Schwartz AJ, Jung I, Colacino JA, Shah YM. Epithelial Hypoxia-Inducible Factor 2alpha Facilitates the Progression of Colon Tumors through Recruiting Neutrophils. *Mol Cell Biol* 2017;**37** e00481–16.

[11] Mladenova DN, Dahlstrom JE, Tran PN, Benthani F, Bean EG, Ng I, Pangon L, Currey N, Kohonen-Corish MR. HIF1alpha deficiency reduces inflammation in a mouse model of proximal colon cancer. *Dis Model Mech* 2015;**8**:1093–103.

[12] Grivennikov SI, Greten FR, Karin M. Immunity, inflammation, and cancer. *Cell* 2010;**140**:883–99.

[13] Sharma V, Collins LB, Chen TH, Herr N, Takeda S, Sun W, Swenberg JA, Nakamura J. Oxidative stress at low levels can induce clustered DNA lesions leading to NHEJ mediated mutations. *Oncotarget* 2016;**7**:25377–90.

[14] Karin M. NF-kappaB as a critical link between inflammation and cancer. *Cold Spring Harb Perspect Biol* 2009;**1**:a000141.

[15] Grivennikov S, Karin E, Terzic J, Mucida D, Yu GY, Vallabhapurapu S, Scheller J, Rose-John S, Cheroutre H, Eckmann L, et al. IL-6 and Stat3 are required for survival of intestinal epithelial cells and development of colitis-associated cancer. *Cancer Cell* 2009;**15**:103–13.

[16] Dolcet X, Llobet D, Pallares J, Matias-Guiu X. NF-kB in development and progression of human cancer. *Virchows Arch* 2005;**446**:475–82.

[17] Luo JL, Maeda S, Hsu LC, Yagita H, Karin M. Inhibition of NF-kappaB in cancer cells converts inflammation- induced tumor growth mediated by TNFalpha to TRAIL-mediated tumor regression. *Cancer Cell* 2004;**6**:297–305.

[18] Colgan SP, Taylor CT. Hypoxia: an alarm signal during intestinal inflammation. *Nat Rev Gastroenterol Hepatol* 2010;**7**:281–7.

[19] Muller-Edenborn K, Leger K, Glaus Garzon JF, Oertli C, Mirsaidi A, Richards PJ, Rehrauer H, Spielmann P, Hoogewijs D, Borsig L, et al. Hypoxia attenuates the proinflammatory response in colon cancer cells by regulating IkappaB. *Oncotarget* 2015;**6**:20288–301.

[20] Hatakeyama M, Opitz L, Russo G, Qi W, Schlapbach R, Rehrauer H. SUSHI: an exquisite recipe for fully documented, reproducible and reusable NGS data analysis. *BMC Bioinform* 2016;**17**:228.

[21] Dobin A, Davis CA, Schlesinger F, Drenkow J, Zaleski C, Jha S, Batut P, Chaisson M, Gingeras TR. STAR: ultrafast universal RNA-seq aligner. *Bioinformatics* 2013;**29**:15–21.

[22] Liao Y, Smyth GK, Shi W. The Subread aligner: fast, accurate and scalable read mapping by seed-and-vote. *Nucleic Acids Res* 2013;**41**:e108.

[23] Love MI, Huber W, Anders S. Moderated estimation of fold change and dispersion for RNA-seq data with DESeq2. *Genome Biol* 2014;**15**:550.

[24] Brown KR, Jurisica I. Online predicted human interaction database. *Bioinformatics* 2005;**21**:2076–82.

[25] Brown KR, Otasek D, Ali M, McGuffin MJ, Xie W, Devani B, Toch IL, Jurisica I. NAViGaTOR: network Analysis, visualization and graphing Toronto. *Bioinformatics* 2009;**25**:3327–9.

[26] Yu G, Wang LG, Han Y, He QY. clusterProfiler: an R package for comparing biological themes among gene clusters. *OMICS* 2012;**16**:284–7.

[27] Durinck S, Spellman PT, Birney E, Huber W. Mapping identifiers for the integration of genomic datasets with the R/Bioconductor package biomaRt. *Nat Protoc* 2009;**4**:1184–91.

[28] Yu G, Wang LG, Yan GR, He QY. DOSE: an R/Bioconductor package for disease ontology semantic and enrichment analysis. *Bioinformatics* 2015;**31**:608–9.

[29] Carmeliet P, Jain RK. Molecular mechanisms and clinical applications of angiogenesis. *Nature* 2011;**473**:298–307.

[30] Pinero J, Ramirez-Anguita JM, Sauch-Pitarch J, Ronzano F, Centeno E, Sanz F, Furlong LI. The DisGeNET knowledge platform for disease genomics: 2019 update. *Nucleic Acids Res* 2020;**48**:D845–55.

[31] Kessenbrock K, Plaks V, Werb Z. Matrix metalloproteinases: regulators of the tumor microenvironment. *Cell* 2010;**141**:52–67.

[32] Baba Y, Nosho K, Shima K, Irahara N, Chan AT, Meyerhardt JA, Chung DC, Giovannucci EL, Fuchs CS, Ogino S. HIF1A overexpression is associated with poor prognosis in a cohort of 731 colorectal cancers. *Am J Pathol* 2010;**176**:2292–301.

[33] Novell A, Martinez-Alonso M, Mira M, Tarragona J, Salud A, Matias-Guiu X. Prognostic value of c-FLIPL/s, HIF-1alpha, and NF-kappabeta in stage II and III rectal cancer. *Virchows Arch* 2014;**464**:645–54.

[34] Babic AM, Kireeva ML, Kolesnikova TV, Lau LF. CYR61, a product of a growth factor-inducible immediate early gene, promotes angiogenesis and tumor growth. *Proc Natl Acad Sci U S A* 1998;**95**:6355–60.

[35] Tsai MS, Bogart DF, Castaneda JM, Li P, Lupu R. Cyr61 promotes breast tumorigenesis and cancer progression. *Oncogene* 2002;**21**:8178–85.

[36] Maity G, Mehta S, Haque I, Dhar K, Sarkar S, Banerjee SK, Banerjee S. Pancreatic tumor cell secreted CCN1/Cyr61 promotes endothelial cell migration and aberrant neovascularization. *Sci Rep* 2014;**4**:4995.

[37] Chen Y, Du XY. Functional properties and intracellular signaling of CCN1/Cyr61. *J Cell Biochem* 2007;**100**:1337–45.

[38] Sun H, Li XB, Meng Y, Fan L, Li M, Fang J. TRAF6 upregulates expression of HIF-1alpha and promotes tumor angiogenesis. *Cancer Res* 2013;**73**:4950–4959.

[39] Rezaeian AH, Li CF, Wu CY, Zhang X, Delacerda J, You MJ, Han F, Cai Z, Jeong YS, Jin G, et al. A hypoxia-responsive TRAF6-ATM-H2AX signalling axis promotes HIF1alpha activation, tumorigenesis and metastasis. *Nat Cell Biol* 2017;**19**:38–51.

[40] Triner D, Shah YM. Hypoxia-inducible factors: a central link between inflammation and cancer. *J Clin Invest* 2016;**126**:3689–98.

[41] Zhong H, De Marzo AM, Laughner E, Lim M, Hilton DA, Zagzag D, Buechler P, Isaacs WB, Semenza GL, Simons JW. Overexpression of hypoxia-inducible factor 1alpha in common human cancers and their metastases. *Cancer Res* 1999;**59**:5830–5.

[42] Greenhough A, Bagley C, Heesom KJ, Gurevich DB, Gay D, Bond M, Collard TJ, Paraskeva C, Martin P, Sansom OJ, et al. Cancer cell adaptation to hypoxia involves a HIF-GPRC5A-YAP axis. *EMBO Mol Med* 2018;**10**:e8699.

[43] Zhang J, Zhu L, Fang J, Ge Z, Li X. LRG1 modulates epithelial-mesenchymal transition and angiogenesis in colorectal cancer via HIF-1alpha activation. *J Exp Clin Cancer Res* 2016;**35**:29.

[44] Campbell EL, Bruyninckx WJ, Kelly CJ, Glover LE, McNamee EN, Bowers BE, Bayless AJ, Scully M, Saeedi BJ, Golden-Mason L, et al. Transmigrating neutrophils shape the mucosal microenvironment through localized oxygen depletion to influence resolution of inflammation. *Immunity* 2014;**40**:66–77.

[45] Wei TT, Lin YT, Tang SP, Luo CK, Tsai CT, Shun CT, Chen CC. Metabolic targeting of HIF-1alpha potentiates the therapeutic efficacy of oxaliplatin in colorectal cancer. *Oncogene* 2020;**39**:414–27.

[46] Rosano S, Cora D, Parab S, Zaffuto S, Isella C, Porporato R, Hoza RM, Calogero RA, Riganti C, Bussolino F, et al. A regulatory microRNA network controls endothelial cell phenotypic switch during sprouting angiogenesis. *Elife* 2020;**9**:e48095.

[47] Jain RK. Normalizing tumor vasculature with anti-angiogenic therapy: a new paradigm for combination therapy. *Nat Med* 2001;**7**:987–9.

[48] Chintalapudi MR, Markiewicz M, Kose N, Dammai V, Champion KJ, Hoda RS, Trojanowska M, Hsu T. Cyr61/CCN1 and CTGF/CCN2 mediate the proangiogenic activity of VHL-mutant renal carcinoma cells. *Carcinogenesis* 2008;**29**:696–703.

[49] Nguyen N, Kuliopulos A, Graham RA, Covic L. Tumor-derived Cyr61(CCN1) promotes stromal matrix metalloproteinase-1 production and protease-activated receptor 1-dependent migration of breast cancer cells. *Cancer Res* 2006;**66**:2658–65.

[50] Espinoza I, Menendez JA, Kvp CM, Lupu R. CCN1 promotes vascular endothelial growth factor secretion through alphavbeta 3 integrin receptors in breast cancer. *J Cell Commun Signal* 2014;**8**:23–7.

[51] Karin M. Nuclear factor-kappaB in cancer development and progression. *Nature* 2006;**441**:431–6.

[52] Greten FR, Eckmann L, Greten TF, Park JM, Li ZW, Egan LJ, Kagnoff MF, Karin M. IKKbeta links inflammation and tumorigenesis in a mouse model of colitis-associated cancer. *Cell* 2004;**118**:285–96.

[53] De Simone V, Franze E, Ronchetti G, Colantoni A, Fantini MC, Di Fusco D, Sica GS, Sileri P, MacDonald TT, Pallone F, et al. Th17-type cytokines, IL-6 and TNF-alpha synergistically activate STAT3 and NF-kB to promote colorectal cancer cell growth. *Oncogene* 2015;**34**:3493–503.

[54] Uronis JM, Muhlbauer M, Herfarth HH, Rubinas TC, Jones GS, Jobin C. Modulation of the intestinal microbiota alters colitis-associated colorectal cancer susceptibility. *PLoS ONE* 2009;**4**:e6026.

[55] Scheeren FA, Kuo AH, van Weele LJ, Cai S, Glykofridis I, Sikandar SS, Zabala M, Qian D, Lam JS, Johnston D, et al. A cell-intrinsic role for TLR2-MYD88 in intestinal and breast epithelia and oncogenesis. *Nat Cell Biol* 2014;**16**:1238–48.

[56] Caballero S, Pamer EG. Microbiota-mediated inflammation and antimicrobial defense in the intestine. *Annu Rev Immunol* 2015;**33**:227–56.

[57] Liang J, Li Z, Li J, Peng C, Dai W, He H, Zeng S, Xie C. Application of IVIM-DWI in Detecting the Tumor Vasculogenic Mimicry Under Antiangiogenesis Combined With Oxaliplatin Treatment. *Front Oncol* 2020;**10**:1376.

[58] Sobecki M, Mrouj K, Camasses A, Parisis N, Nicolas E, Lleres D, Gerbe F, Prieto S, Krasinska L, David A, et al. The cell proliferation antigen Ki-67 organises heterochromatin. *Elife* 2016;**5**:e13722.

[59] Noble P, Vyas M, Al-Attar A, Durrant S, Scholefield J, Durrant L. High levels of cleaved caspase-3 in colorectal tumour stroma predict good survival. *Br J Cancer* 2013;**108**:2097–105.

[60] Ogane N, Yasuda M, Kato H, Kato T, Yano M, Kameda Y, Kamoshida S. Cleaved caspase-3 expression is a potential prognostic factor for endometrial cancer with positive peritoneal cytology. *Cytopathology* 2018;**29**:254–61.

[61] Liu X, Liu B, Li R, Wang F, Wang N, Zhang M, Bai Y, Wu J, Liu L, Han D, et al. miR-146a-5p Plays an oncogenic role in NSCLC via suppression of TRAF6. *Front Cell Dev Biol* 2020;**8**:847.

[62] Bradley JR, Pober JS. Tumor necrosis factor receptor-associated factors (TRAFs. *Oncogene* 2001;**20**:6482–91.

[63] Zhu G, Lin C, Cheng Z, Wang Q, Hoffman RM, Singh SR, Huang Y, Zheng W, Yang S, Ye J. TRAF6-mediated inflammatory cytokines secretion in LPS-induced colorectal cancer cells is regulated by miR-140. *Cancer Genom Proteom* 2020;**17**:23–33.

[64] Luo Z, Zhang X, Zeng W, Su J, Yang K, Lu L, Lim CB, Tang W, Wu L, Zhao S, et al. TRAF6 regulates melanoma invasion and metastasis through ubiquitination of Basigin. *Oncotarget* 2016;**7**:7179–92.

[65] Zapata JM, Krajewska M, Krajewski S, Kitada S, Welsh K, Monks A, McCloskey N, Gordon J, Kipps TJ, Gascoyne RD, et al. TNFR-associated factor family protein expression in normal tissues and lymphoid malignancies. *J Immunol* 2000;**165**:5084–96.

Supplementary Data

Glaus Garzon et al.

Tumor cell endogenous HIF-1α activity induces aberrant angiogenesis and interacts with TRAF6 pathway required for colorectal cancer development

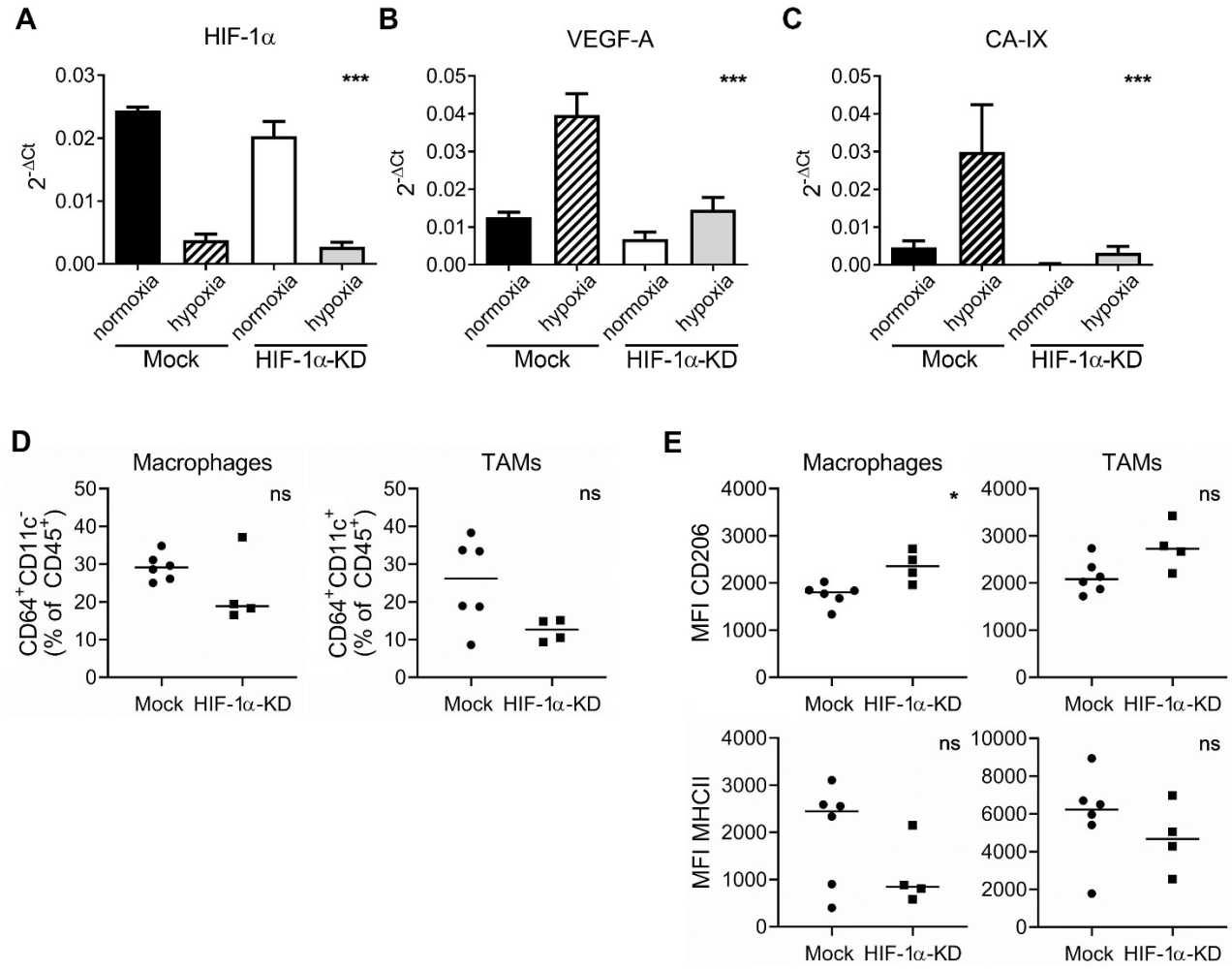

Supplementary Figure 1. Characterization of HIF-1α-KD MC-38 cells. A) Transcript levels of HIF-1α were determined by qPCR after 8 hours incubation under normoxia (21% O_2) or hypoxia (0.2% O_2) stimulation. The expression levels of canonical HIF target genes VEGF-A **(B)** and CA-IX **(C)** were quantified by RT-qPCR after 8 hours incubation under normoxia (21% O_2) or hypoxia (0.2% O_2) compared to mock controls. Expression levels were normalized to constitutively expressed ribosomal protein S12 mRNA levels. **(D)** Number of macrophages ($CD64^+/CD11c^-$) and tumor-associated macrophages - TAMs ($CD64^+/CD11c^+$) in orthotopic tumors represented as percentage of living $CD45^+$ cells, determined by flow cytometry. (**E)** Cell surface expression of polarization markers MHCII and CD206 was analyzed by flow cytometry, in parallel to the experiments shown under D. MFI from FMO control was subtracted from each sample; MFI, median fluorescence intensity. Statistical significance was assessed using the Mann-Whitney test;). *, $p < 0.05$; ***, $p < 0.001$.

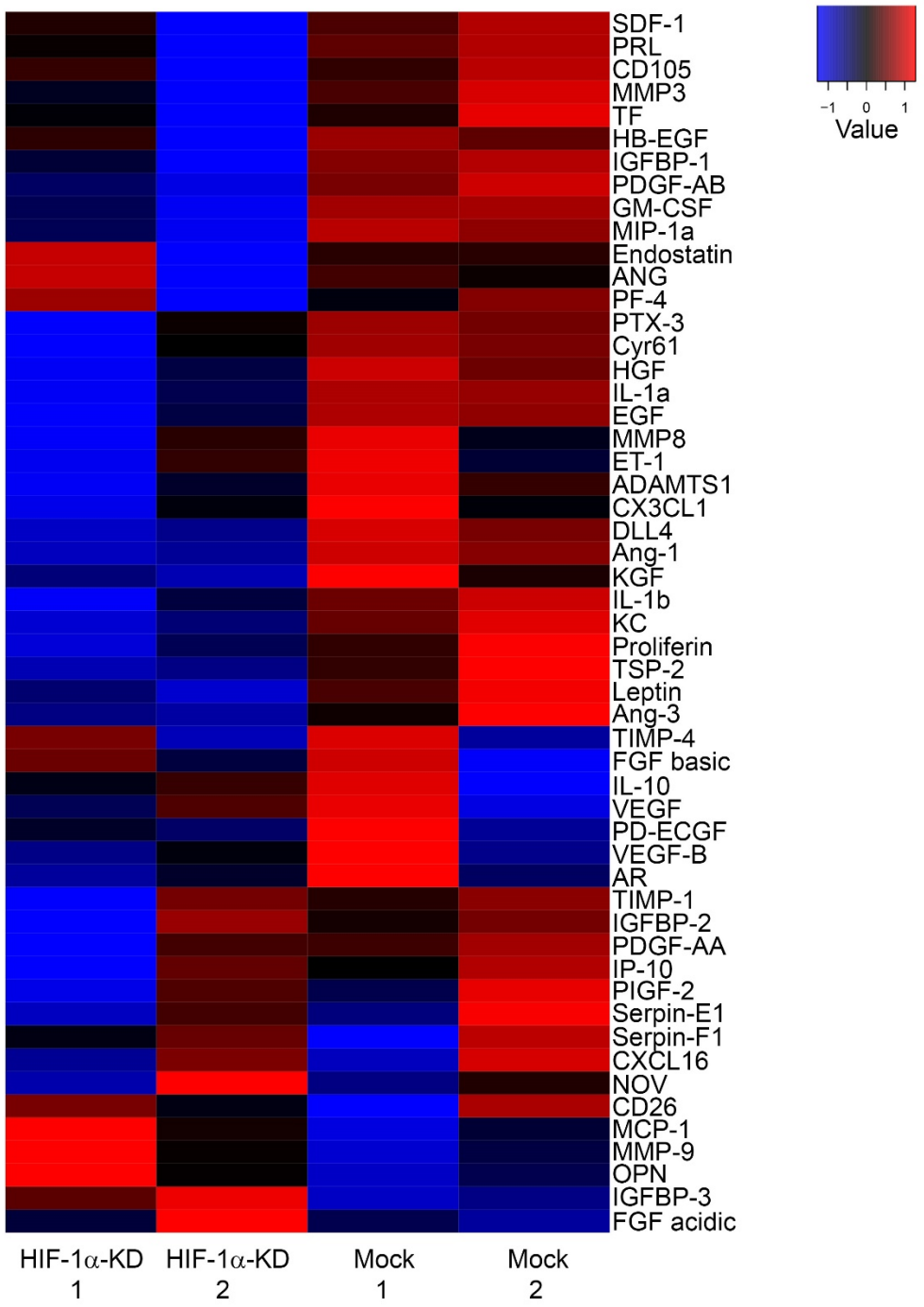

Supplementary Figure 2. Angiogenesis protein arrays of tumor lysates from HIF-1α KD and Mock cecal tumors. Total tumor lysates incubated on Angiogenesis Array. Dot blot pixel densities were quantified and normalized to internal manufacturer's control and plotted as heatmap using web application from Functional Genomic Center Zurich.

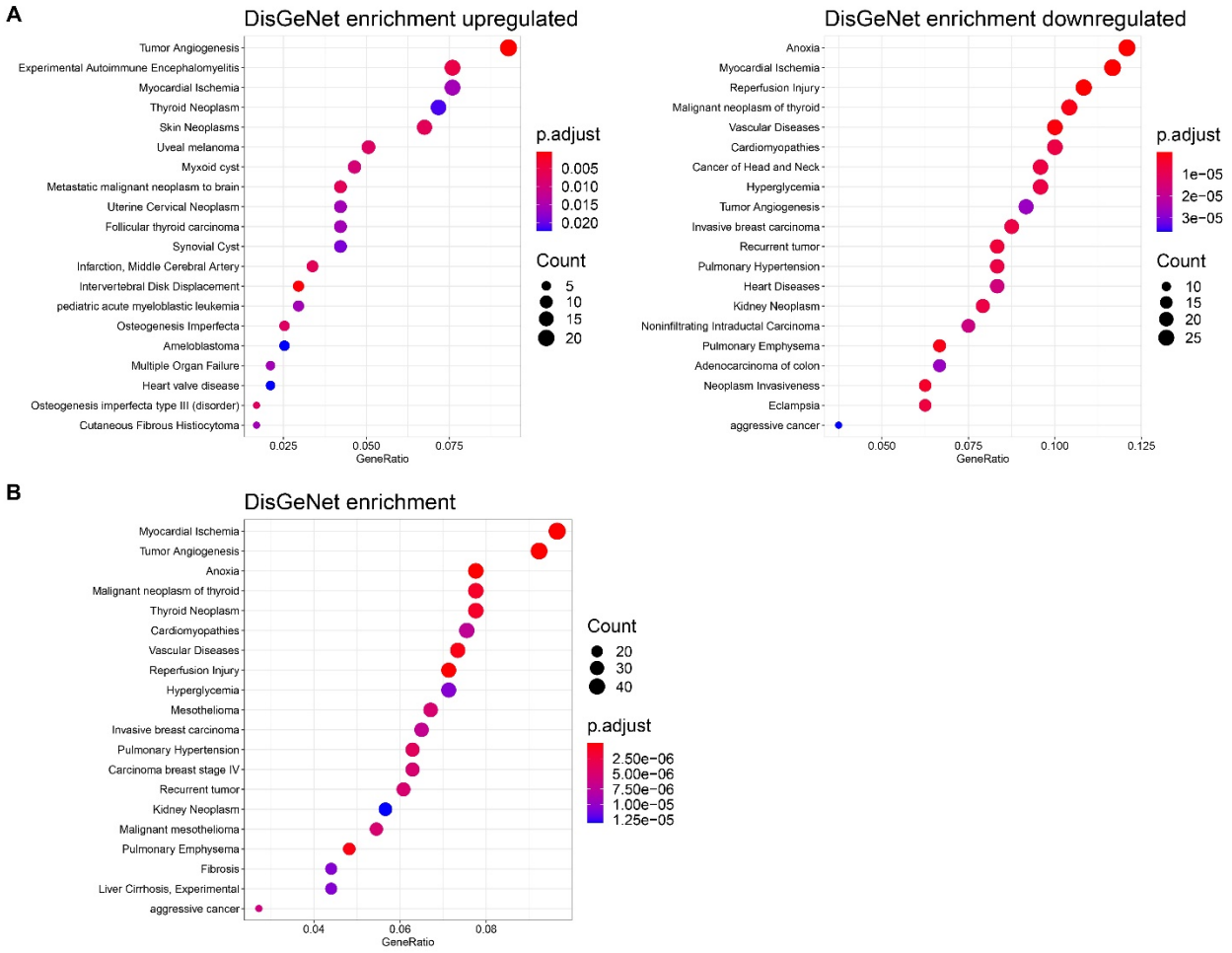

Supplementary Figure 3. Disease enrichment analysis of genes using human curated sets. **A)** List of genes from MC-38 HIF-1a KD cells versus Mock cells sorted from intracecal tumors were converted to human symbols and used for disease enrichment analysis using DOSE_3.14.0, using DisGeNet (DGN) dataset. Plots were obtained using clusterProfiler

A

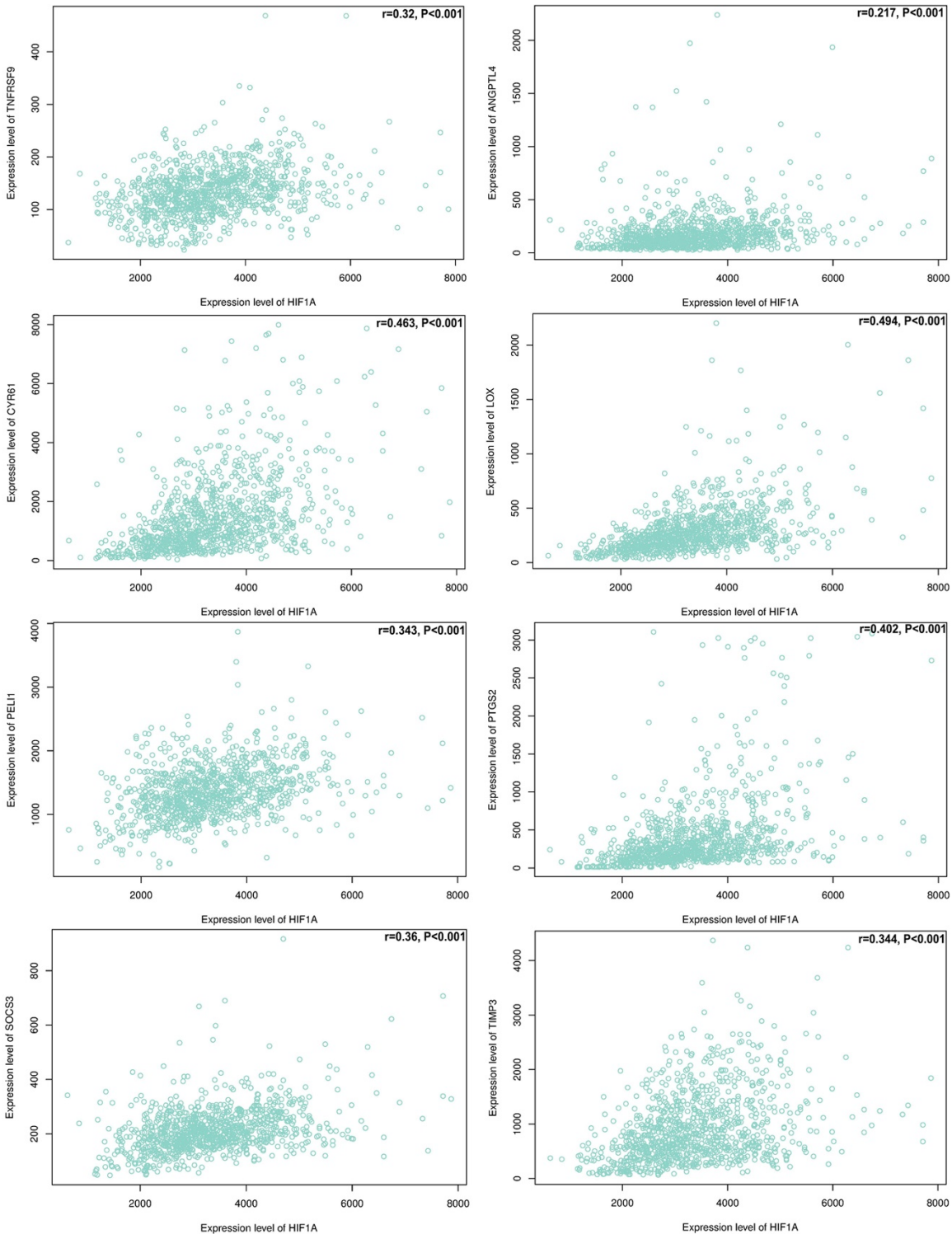
r=0.32, P<0.001
Expression level of TNFRSF9
Expression level of HIF1A
r=0.217, P<0.001
Expression level of ANGPTL4
Expression level of HIF1A
r=0.463, P<0.001
Expression level of CYR61
Expression level of HIF1A
r=0.494, P<0.001
Expression level of LOX
Expression level of HIF1A
r=0.343, P<0.001
Expression level of PELI1
Expression level of HIF1A
r=0.402, P<0.001
Expression level of PTGS2
Expression level of HIF1A
r=0.36, P<0.001
Expression level of SOCS3
Expression level of HIF1A
r=0.344, P<0.001
Expression level of TIMP3
Expression level of HIF1A

B

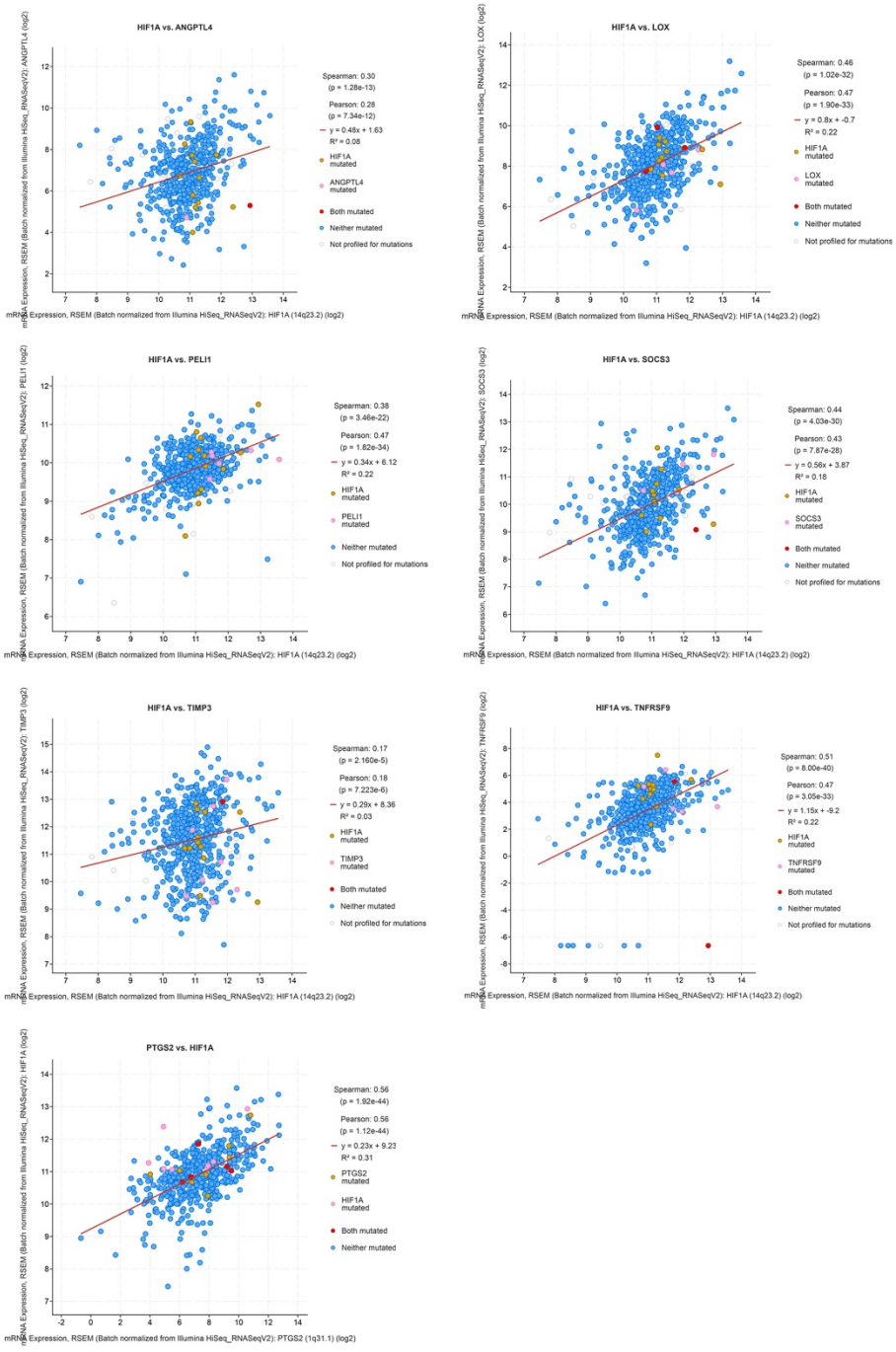

Supplementary Figure 4. HIF-1α expression in clinical samples correlates with genes downregulated in HIF-KD sorted tumor cells. A) Correlation plots were drawn using the webtool In Silico Transcriptomics Ver. 2.1.3. (http://ist.medisapiens.com), focusing on 991 human colorectal cancer samples. All results were significant ($p < 0.001$) and positively correlated ($r > 0.2$). **B)** Correlation plots using 594 colorectal cancer patient samples from Colorectal Adenocarcinoma dataset (TCGA, PanCancer Atlas; https://www.cbioportal.org/ ver. 3.4.3).

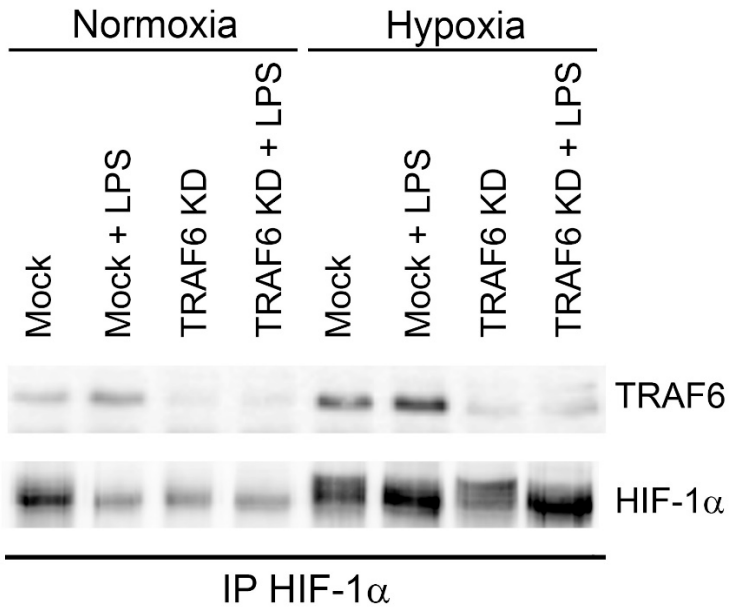

Supplementary Figure 5. HIF-1α immunoprecipitation followed by TRAF-6 detection in murine colon carcinoma cell line MC-38 cells. Immunoprecipitation of HIF-1α in Mock and TRAF6-KD MC-38 cells, which were detected either with TRAF6 or HIF-1α Ab, respectively (n =3). Cells were incubated for 8 hours under normoxia (21% O_2) or hypoxia (0.2% O_2). Additionally, cells were stimulated with 1 μg/mL LPS for one hour either under normoxia or hypoxia.

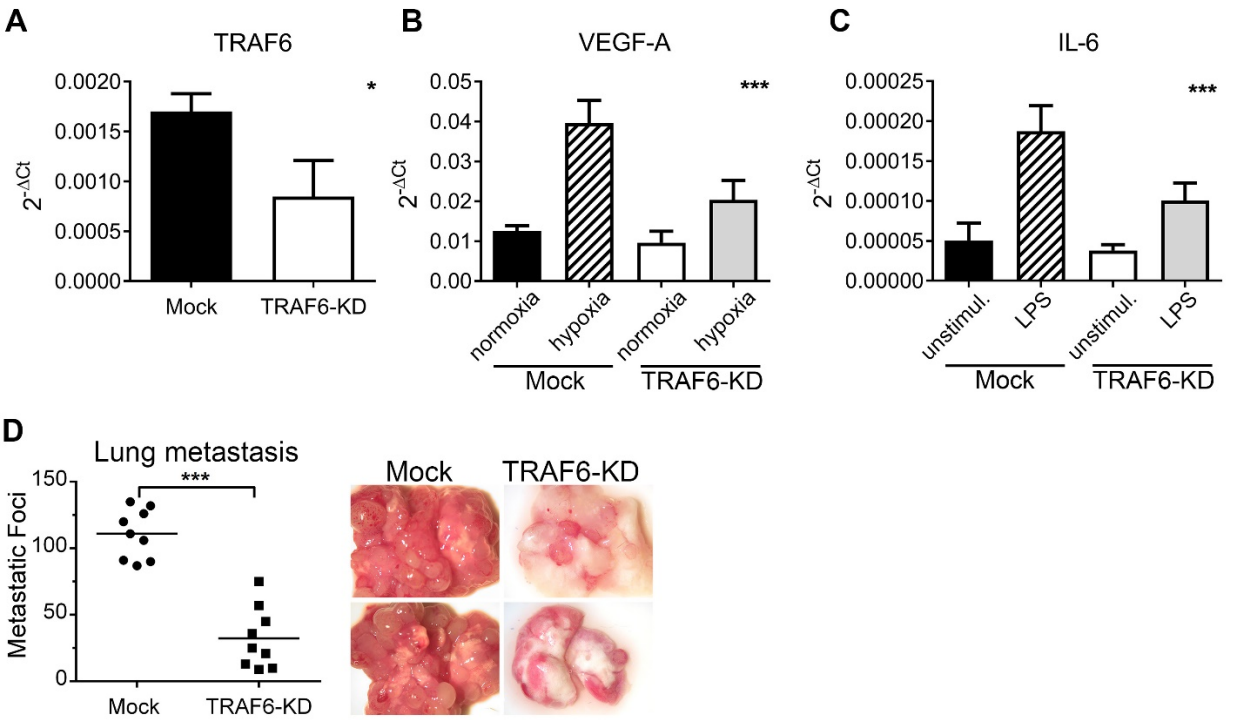

Supplementary Figure 6. Characterization of TRAF6-KD MC-38 cells. A). Transcript levels of TRAF6 were determined by RT-qPCR. mRNA expression levels of VEGF-A **(B)** and canonical TRAF6 target gene IL-6 **(C)** were quantified by RT-qPCR after LPS stimulation (1 μg/mL, 1 hour) compared to mock control and unstimulated cells. Expression levels were normalized to constitutively expressed ribosomal protein S12 mRNA levels. **D)** Experimental lung metastasis of Mock and TRAF6-KD MC-38 cells together with representative images of lung tumors after 28 days of i.v. injection. Mice from two independent experiments are presented. Statistical significance was assessed using the Mann-Whitney test; *, $p < 0.05$; ***, $p< 0.001$.

Supplemental experimental procedures

Angiogenesis Array

Perfused tumors were homogenized in 350 µl PBS containing protease inhibitors (complete EDTA-free, Roche) by using a Polytron (Brinkhan). Samples were spun down (15,000 x g for 15 min at 4°C), supernatant was separated, and protein concentration was determined by BCA assay. Tumor lysate (400 µg) was incubated on a membrane spotted with the Mouse Angiogenesis Antibody Array (R&D Systems). Upon development, pixel density was analyzed with ImageQuant (GE Healthcare Life Sciences). Background signal density was subtracted and normalized to average density of reference spots. Up- and down-regulation of angiogenic factors was analyzed with a R-based web application developed at the Functional Genomics Center Zurich (http://fgcz-shiny.uzh.ch/fgcz_heatmap_app/).

Experimental metastasis

Mice were intravenously (i.v.) injected with 300,000 MC-38GFP Mock or TRAF6-KD cells. Mice were sacrificed after 28 days and lungs were perfused with PBS. The number of metastatic foci per lung was determined macroscopically by a blinded investigator.

RT-qPCR

Total cellular RNA was extracted using TRI Reagent (Sigma) or RNeasy Plus Mini Kit (Qiagen) following manufacturer's recommendations. cDNA was synthesized from 1 μg of total RNA using Omniscript RT Kit (Qiagen). Quantitative qPCR was performed using KAPA SYBR Green Master Mix (Sigma) on a CFX96 Real-Time System (Biorad). Primers were purchased from Microsynth.

Primer	Sequence
HIF-1a forward	5'-CATCCATGTGACCATGAGGA-3'
HIF-1a reverse	5'-CACGTTGCTGACTTGATGTT-3'
VEGF-A forward	5'-GTACCTCCACCATGCCAAGT-3'
VEGF-A reverse	5'-TCTCGTCGGGGTACTCCTGG-3'
CA-IX (Car9) forward	5'-GCCGCTACTACCGATATGAA-3'
CA-IX (Car9) reverse	5'-CACAAGGAAACGGAGAGAGT-3'
TRAF6 forward	5'-TCATCAGAGAACAGATGCCTAAT-3'
TRAF6 reverse	5'-TCATGTGCAACTGGGTATTCT-3'
IL-6 forward	5'-GTGGAAATGAGAAAAGAGTTGTGC-3'
IL-6 reverse	5'-ACCAGAGGAAATTTTCAATAGGC-3'
Cyr61 forward	5'-AGAGGCTTCCTGTCTTTGG-3'
Cyr61 reverse	5'-CACTCTGGGTTGTCATTGGT-3'
Pdgfa forward	5'-GATGAGGACCTGGGCTTGC-3'
Pdgfa reverse	5'-TCAGCCCCTACGGAGTCTATC-3'
Cox2 forward	5'-ACTGGGCCATGGAGTGGA-3'
Cox2 reverse	5'-GAGTGTCTTTGACTGTGGGGG-3'
Tnfrsf9 forward	5'-GCTGCCCTGAGATCGAAA-3'
Tnfrsf9 reverse	5'-GAAAGTACCAGGCTGACAGTTA-3'
S12 forward	5'-ACGTCAACACTGCTCTACAA-3'
S12 reverse	5'-CTCCACCAGCTTGACATACA-3'

Table 1. Differently regulated genes in sorted HIF-KD tumor cells vs. sorted Mock cells.

Upregulated genes

Gene	log2 Ratio	p Value	Gene	log2 Ratio	p Value	Gene	log2 Ratio	p Value
Arsi	1.536	1.95E-08	*Has2*	0.7751	0.004355	*Gm20489*	0.6574	0.006045
Enpp2	1.515	3.13E-09	*Etv1*	0.7745	0.000191	*Il1b*	0.6566	0.01597
Map1a	1.462	3.08E-08	*Tnfrsf21*	0.7729	0.000628	*Cenpe*	0.6563	0.01369
Col18a1	1.343	2.56E-08	*Stard10*	0.7709	0.004949	*Kirrel3*	0.6562	0.0138
Khdrbs3	1.239	3.55E-06	*Ptpn3*	0.7693	0.001993	*Chd5*	0.6556	0.01661
Tmem54	1.234	1.54E-06	*Ptpn6*	0.7674	0.003255	*Efnb1*	0.6549	0.006815
Nol3	1.168	1.57E-05	*Sytl4*	0.7672	0.004688	*Srpx*	0.6547	0.004553
Lrrc15	1.151	2.45E-05	*Cspg4*	0.7628	0.003232	*Mast2*	0.6531	0.002916
Pcsk9	1.11	3.54E-06	*Plxnd1*	0.7598	0.000469	*Zbed4*	0.6531	0.009298
Fas	1.106	4.91E-06	*Rbm19*	0.7595	0.000418	*Camsap1*	0.6519	0.000963
Stmn2	1.104	5.38E-05	*Ednra*	0.759	0.004118	*Akap13*	0.6518	0.003915
Arap3	1.096	1.47E-05	*Bcas1*	0.7585	0.001786	*Ptpn13*	0.6504	0.01112
Slc15a3	1.086	6.18E-06	*Dkk2*	0.7578	0.002947	*Heg1*	0.6492	0.001532
Hs6st1	1.082	8.08E-07	*Gm6880*	0.7522	0.001189	*Sertad4*	0.648	0.002755
Ston2	1.069	4.03E-05	*Pogk*	0.7514	1.39E-05	*Gm684*	0.647	0.01785
Wfdc12	1.063	8.14E-05	*Gdpd5*	0.7507	0.002728	*Spef1*	0.6461	0.01251
Tenm3	1.06	2.04E-05	*Unc5b*	0.7486	0.001513	*S1pr1*	0.6457	0.003973
Card10	1.057	0.000102	*Macf1*	0.7476	0.001448	*Ccr2*	0.6437	0.01544
Duox1	1.022	0.000161	*Apol6*	0.7464	0.006062	*Kctd12*	0.6436	0.01719
Chst2	1.015	2.25E-05	*Tep1*	0.7463	0.004387	*Gfra2*	0.6431	0.005127
Mdn1	1.001	2.02E-05	*Cep290*	0.7453	0.005887	*Dock4*	0.6424	0.003511
Col2a1	0.9928	0.000176	*Rgl1*	0.7432	0.003597	*Nav1*	0.6419	0.002911
Afap1l2	0.9886	5.15E-05	*Kif26b*	0.7411	0.000364	*Abca1*	0.6418	0.001482
Fam198b	0.9873	0.000312	*Dagla*	0.7402	0.001675	*Zfml*	0.641	0.001805
Extl1	0.985	1.16E-05	*Akap9*	0.74	0.004829	*Ssh2*	0.6406	0.002281
Camk2a	0.9764	0.000325	*Gbp5*	0.7381	0.006021	*Stat4*	0.639	0.01567
Arhgap26	0.9761	1.47E-05	*Ryr2*	0.738	0.006528	*Cd276*	0.6384	0.000482
Prodh	0.9698	9.07E-05	*Ncam1*	0.7365	0.004315	*Abi3bp*	0.6369	0.01008
Serpinf1	0.9674	1.08E-07	*Nin*	0.7331	0.00072	*Pcyox1l*	0.6365	0.01231
Slc22a23	0.9619	0.000451	*Lama4*	0.7304	0.006208	*Myh3*	0.6361	0.01906
Nid2	0.9604	0.000284	*Arid5a*	0.73	0.002825	*Fbln5*	0.6351	0.01692
Aldh1a3	0.9577	0.000477	*Adgra3*	0.7294	0.000428	*C1qtnf1*	0.6347	0.01604

Ttn	0.9508	0.000385	*Car14*	0.7294	0.007353	*Slc26a9*	0.6333	0.01604
2900026A02Rik	0.9474	0.000179	*Neto2*	0.7267	0.001744	*Slitrk5*	0.6314	0.02081
Ptn	0.9462	0.000295	*Zfp600*	0.7254	0.003771	*Fgfr3*	0.63	0.02071
Icam1	0.9447	0.000345	*Tex13*	0.7242	0.00038	*Rgs5*	0.6283	0.02132
Dppa2	0.9439	4.25E-05	*Myo18a*	0.723	0.001961	*Hip1*	0.624	0.003119
Gxylt2	0.9403	0.000157	*Ciita*	0.7177	0.003535	*Zfc3h1*	0.6232	0.004891
Cyp7b1	0.9345	0.000267	*Nckap5*	0.7155	0.009098	*Eml5*	0.6227	0.02289
Cd200	0.9345	0.000439	*Pstpip2*	0.7143	0.008768	*Uhrf1bp1*	0.6222	0.00068
Apcdd1	0.9304	0.000658	*Tcn2*	0.714	0.002885	*Dennd3*	0.6222	0.01726
Scml4	0.9222	0.000547	*Plxnb1*	0.7139	0.002781	*Wisp1*	0.6217	0.001894
Mdfi	0.9219	0.000647	*Cep162*	0.7117	0.00327	*Apobr*	0.6217	0.007581
Ctxn1	0.9142	0.000354	*Nhs*	0.7106	0.009585	*Lpar1*	0.6199	0.01469
Gli1	0.9086	0.000273	*Atp2b4*	0.7098	0.005786	*Golga3*	0.6197	0.001715
Xylt1	0.9067	0.000615	*Nlrc5*	0.7096	0.00061	*Creb3l1*	0.6192	0.01968
Mid1	0.8983	4.39E-05	*Chrnd*	0.7068	0.005292	*Urb1*	0.6184	0.001338
Sorcs2	0.8877	0.000265	*Crip1*	0.7064	0.00975	*Sh3pxd2a*	0.6182	0.004064
Ank1	0.8854	0.000269	*Xlr4b*	0.7056	0.007636	*Dab2*	0.6179	0.007381
Ceacam20	0.8782	0.00047	*Prokr1*	0.7042	0.009533	*Col27a1*	0.6173	0.01624
Spib	0.8771	0.001236	*Slfn9*	0.7029	0.001994	*Nfkbie*	0.6165	0.003431
Mov10l1	0.8757	0.001091	*Apc*	0.702	0.000794	*Gfpt2*	0.6162	0.02175
Bace2	0.8751	0.000619	*Slc16a9*	0.7007	0.0106	*Ankrd26*	0.6154	0.005389
Pgbd5	0.8729	0.001324	*Ankrd11*	0.6984	0.006901	*Tmem173*	0.615	0.001167
Lama5	0.8723	7.65E-05	*Arap2*	0.6976	0.01055	*Penk*	0.6145	0.0161
Slc4a5	0.872	0.00141	*Tvp23a*	0.6949	0.005427	*Ccdc24*	0.6142	0.00579
Tspan2	0.8641	0.001211	*Fyco1*	0.6929	0.001719	*Gm13151*	0.6134	0.02535
Amigo2	0.8617	0.000136	*Lbx1*	0.689	0.00907	*Serpina3f*	0.6131	0.0152
Crb2	0.8587	0.00113	*2010005H15Rik*	0.689	0.012	*Myo1e*	0.6129	0.005001
Golgb1	0.8541	0.001176	*Bcl2*	0.6878	0.004286	*Abca13*	0.6127	0.01598
Prune2	0.8463	5.17E-06	*Cd9*	0.6875	0.00227	*Rgma*	0.6122	0.01227
Slamf8	0.843	0.000239	*Rabl6*	0.687	0.00023	*Wnt6*	0.6121	0.02132
Col3a1	0.841	5.03E-05	*Adamtsl3*	0.6864	0.00092	*Tlr12*	0.6115	0.02116
Cd248	0.8396	0.000449	*Dppa4*	0.6861	0.01066	*Baz1b*	0.6106	0.000965
Zbtb40	0.839	0.000141	*Lynx1*	0.6855	0.005872	*Synj2*	0.6095	0.003389
Map3k5	0.8384	0.000552	*Tmem2*	0.6848	0.00245	*Slit2*	0.6092	0.001397
Mlph	0.8372	0.000556	*Il2rg*	0.684	0.004172	*Sema4a*	0.6087	0.01751
Bptf	0.8289	0.000474	*Gm13145*	0.6822	0.002066	*Zfp251*	0.608	0.00658

Plxna1	0.8279	0.000332	*Scara5*	0.6821	0.005129	*Dennd2a*	0.6078	0.00335
Vegfc	0.826	0.001686	*Gdf11*	0.6818	0.000524	*Thbs2*	0.6078	0.01377
Notch1	0.8257	0.000457	*Flrt2*	0.6817	0.003201	*P2rx7*	0.6076	0.01264
Mmp28	0.823	0.000812	*Slpi*	0.6802	0.006398	*Tmem159*	0.6076	0.02675
Casp8ap2	0.8171	0.000276	*Mtcl1*	0.6797	0.01184	*Spata13*	0.6048	0.01287
Slx4	0.8147	0.000411	*Itga1*	0.679	0.01299	*Akna*	0.6026	0.01763
Plxna2	0.8112	0.000271	*Pid1*	0.6777	0.006235	*Flrt3*	0.6013	0.02414
Gm15386	0.8108	0.002021	*Tph2*	0.6777	0.01221	*Cntrl*	0.6009	0.02364
Sema6a	0.8078	0.00179	*Gareml*	0.6763	0.01362	*Sema3c*	0.5988	0.02472
Hsph1	0.8065	4.91E-05	*Golga4*	0.6755	0.007958	*Wdfy3*	0.5976	0.004101
Ccdc36	0.8054	0.002731	*Fat4*	0.6754	0.006058	*Grip1*	0.5972	0.0281
Rorb	0.8051	0.002187	*Trak2*	0.6751	0.000293	*Col11a2*	0.5947	0.02764
Abca3	0.805	0.003169	*Col1a1*	0.6743	0.01253	*Slc2a13*	0.5941	0.01877
Pde2a	0.8045	0.002227	*Syne2*	0.674	0.008263	*Uchl1*	0.5938	0.0213
Trpa1	0.7991	0.002311	*Rps6kc1*	0.6714	0.005068	*Trim56*	0.5928	0.007752
Zfp936	0.7985	0.003183	*Chd7*	0.6703	0.0145	*Lck*	0.5928	0.02781
Trip11	0.7963	0.000364	*A4galt*	0.6693	0.01468	*Bdp1*	0.5927	0.007637
Col5a2	0.7926	0.000193	*Nov*	0.6667	0.005249	*Lgi4*	0.5925	0.02681
Cd38	0.7915	0.000715	*Magi1*	0.6663	0.01477	*St3gal1*	0.5923	0.007066
Tmem119	0.7903	0.00275	*Gli2*	0.6633	0.01559	*Tnrc6c*	0.592	0.01445
Spry1	0.79	0.003254	*Nipbl*	0.6615	0.001738	*Serpinh1*	0.5919	0.01216
Amot	0.7884	0.000381	*Tcf20*	0.6602	0.002459	*Ccne1*	0.5915	0.007431
Fjx1	0.7831	0.003726	*Pprc1*	0.6595	0.001264	*C2cd2*	0.5905	0.006618
Lbp	0.7794	0.003456	*Nol4l*	0.6586	0.01597	*Lamc1*	0.5902	0.003146
Pdgfa	0.7786	0.0003	*Ccr7*	0.6578	0.01648	*Fam212b*	0.5901	0.0109
Cntnap4	0.776	0.004216						

Downregulated genes

Gene	log2 Ratio	p Value	Gene	log2 Ratio	p Value	Gene	log2 Ratio	p Value
Tmem218	-0.5912	0.008697	*Sorbs3*	-0.6919	0.000315	*Pgam1*	-0.9223	1.69E-09
Nusap1	-0.5912	0.01872	*Ctla2a*	-0.6923	0.004933	*Plac8*	-0.9269	8.39E-06
Rpl36	-0.5924	0.009233	*Gpr146*	-0.6931	0.002179	*Wwc1*	-0.9277	0.00068
Deptor	-0.5941	0.02758	*Hbegf*	-0.6945	0.004465	*Cdh17*	-0.9292	0.000614
Cd109	-0.5947	0.01985	*Amotl2*	-0.6951	0.005257	*Pttg1ip*	-0.9315	1.50E-06
Nmrk1	-0.5949	0.006166	*Galnt13*	-0.6961	0.01007	*Bhlhe40*	-0.932	5.69E-06
Cdkn2d	-0.5956	0.00502	*S100a3*	-0.6971	0.009731	*Hist1h1c*	-0.9428	0.000132
Tinagl1	-0.5958	0.02542	*Sgcd*	-0.6979	0.01064	*Cdkn1b*	-0.9468	1.34E-06
Alkbh5	-0.596	0.00065	*Upk1b*	-0.6985	0.00771	*Junb*	-0.9502	0.00017
Akap7	-0.596	0.007963	*Pqlc3*	-0.6997	0.002683	*Mfsd9*	-0.9629	0.000182
Cyp4v3	-0.597	0.009686	*Galk1*	-0.703	0.000106	*3110057O12Rik*	-0.9651	0.00021
Ppp1r3b	-0.5979	0.02211	*Map2k1*	-0.7097	6.11E-05	*Foxc2*	-0.9682	0.000248
Klf10	-0.5983	0.005653	*Timp3*	-0.7115	0.007006	*Fabp5*	-0.9747	2.12E-05
Eps8l2	-0.5988	0.001111	*Usp53*	-0.7147	0.002861	*Klf6*	-0.9787	1.06E-05
Hpse	-0.5991	0.001167	*Msln*	-0.7186	0.006922	*Ampd3*	-0.9804	9.13E-07
Pxmp4	-0.6003	0.008968	*Srd5a2*	-0.719	0.007495	*Tpi1*	-0.9825	1.33E-10
Slc37a4	-0.6015	0.001067	*G2e3*	-0.7195	0.001169	*Gpi1*	-0.9833	1.12E-08
B630005N14Rik	-0.6016	0.003596	*Als2cr12*	-0.7218	0.008446	*Gapdh*	-1.003	4.01E-10
Ccdc109b	-0.6043	0.002009	*Hif1a*	-0.7225	0.008222	*U90926*	-1.014	0.000214
Sat1	-0.6044	0.002473	*Neurl2*	-0.7227	0.004352	*Sertad1*	-1.018	1.33E-07
Lxn	-0.6044	0.01426	*Pdk3*	-0.725	6.28E-05	*Serpine1*	-1.018	2.55E-06
Adm	-0.6054	0.02169	*Tcp11l2*	-0.7253	0.007003	*Nos2*	-1.02	9.96E-05
Rps10	-0.6055	0.001354	*Dyrk4*	-0.7254	0.008133	*Maff*	-1.023	1.50E-06

Cdc42ep2	-0.6075	0.000723	*Cda*	-0.7294	0.000239	*Egr2*	-1.024	6.83E-05
Rapsn	-0.6083	0.02147	*Rpl22l1*	-0.731	0.001717	*Mctp2*	-1.027	0.00016
Id3	-0.6083	0.02287	*Gria4*	-0.7364	0.001079	*Prdm1*	-1.035	0.000148
Hbp1	-0.6086	0.003932	*Pfkp*	-0.7375	2.31E-05	*Klk1b27*	-1.036	3.95E-05
Islr2	-0.6092	0.02606	*Slc2a8*	-0.7389	0.000931	*Acsbg1*	-1.041	8.02E-05
Rps24	-0.611	0.002705	*Pcgf5*	-0.74	4.11E-05	*Ldha*	-1.043	2.83E-10
Arrdc3	-0.6111	0.001487	*Slc16a6*	-0.74	0.003221	*Hist1h2bc*	-1.047	5.91E-06
Ftl1	-0.612	0.000445	*Txnip*	-0.7472	0.000728	*Aldoc*	-1.048	0.000127
Dnajc5	-0.6123	0.000367	*Klra4*	-0.7472	0.00223	*Ramp3*	-1.051	0.000127
AC136513.6	-0.6126	0.001234	*Plekha2*	-0.7487	6.29E-05	*Epha7*	-1.055	0.000115
Tpt1	-0.6157	0.00177	*Klhl24*	-0.7532	0.000956	*Aire*	-1.057	7.96E-05
Rassf7	-0.6157	0.007976	*Rundc3b*	-0.7536	0.002259	*Ephx1*	-1.058	3.58E-06
Vim	-0.6195	4.68E-05	*Casp12*	-0.7573	0.00143	*Slc16a3*	-1.059	6.22E-09
Eid1	-0.6208	0.002794	*Pkm*	-0.7628	3.64E-07	*Fgf7*	-1.065	1.42E-05
Ube2e2	-0.6219	0.003813	*Socs3*	-0.7643	0.000455	*Zfp36*	-1.069	2.74E-05
Klf9	-0.6236	0.008532	*Hspb6*	-0.7665	0.000453	*Aldoa*	-1.083	3.13E-10
Pik3ip1	-0.6249	0.004236	*Eno1*	-0.7693	3.88E-06	*Hacd2*	-1.093	3.43E-07
Rusc2	-0.6252	0.009511	*Pik3cb*	-0.7709	0.000114	*Lox*	-1.094	4.97E-05
Homer1	-0.6266	0.002161	*Nampt*	-0.7743	4.03E-05	*Klf11*	-1.102	1.12E-06
Insig2	-0.628	0.001689	*Fam46b*	-0.7752	0.00352	*Pfkl*	-1.108	1.43E-09
Nicn1	-0.6281	0.002307	*Mturn*	-0.7782	0.004539	*Car9*	-1.109	4.54E-05
Cryl1	-0.6339	0.01577	*Nxph4*	-0.782	0.002749	*Ier2*	-1.114	6.95E-07
Trim17	-0.634	0.007392	*Hist3h2a*	-0.7823	0.000559	*Frat2*	-1.137	2.11E-05
Hk1	-0.6345	5.64E-05	*Ndufv3*	-0.7826	6.38E-07	*Lrrn4cl*	-1.138	1.08E-06
Cnr1	-0.635	0.007941	*Lgals3*	-0.7834	0.00076	*Higd1a*	-1.164	5.21E-09

Myl9	-0.6363	0.01413	*Tiparp*	-0.7899	0.000286	*Pgm2*	-1.168	2.82E-11
Peli1	-0.6371	0.0107	*Pnrc1*	-0.7907	0.000618	*Mxi1*	-1.171	1.47E-10
Cyp2d22	-0.6375	0.004964	*Dmxl1*	-0.7911	0.000796	*Crebrf*	-1.175	2.39E-06
Eef2	-0.638	0.00011	*Hoga1*	-0.7927	0.001347	*Rhob*	-1.185	6.83E-08
Ugdh	-0.6381	0.000254	*Il13ra2*	-0.7933	0.003739	*Hlf*	-1.209	9.88E-06
Inpp5k	-0.6393	0.003238	*Ddit4*	-0.7973	8.55E-06	*Mgarp*	-1.211	2.93E-09
Gsto2	-0.6397	0.01707	*Sgk1*	-0.801	4.59E-05	*Jund*	-1.214	7.84E-08
Dffb	-0.6406	0.008095	*Tmem171*	-0.803	0.003157	*Sap30*	-1.219	6.04E-10
Cdh5	-0.6411	0.004012	*Mif*	-0.8049	6.88E-05	*Itpk1*	-1.235	4.57E-11
Me2	-0.643	0.000158	*Elovl7*	-0.8071	0.000132	*Celf2*	-1.241	2.31E-08
Nsun3	-0.6436	0.00725	*Jun*	-0.8105	0.000443	*Ak4*	-1.256	1.62E-11
Otud1	-0.6439	0.01015	*Lrrn3*	-0.812	0.002258	*Klf2*	-1.261	1.78E-07
Itgb7	-0.6442	0.006606	*Fhl2*	-0.8138	0.000196	*Ciart*	-1.273	5.47E-08
Spg21	-0.6447	0.000738	*Cyr61*	-0.817	0.000687	*Gys1*	-1.279	3.36E-14
Lactb2	-0.6447	0.001587	*Ptgs2*	-0.825	3.91E-05	*Prelid2*	-1.299	6.46E-10
Agl	-0.6488	0.001925	*Cirbp*	-0.8266	0.000188	*Angptl4*	-1.326	6.60E-07
Gpr137b	-0.6504	0.002221	*Medag*	-0.8282	0.000417	*Ppp1r3c*	-1.326	1.09E-06
Prkab2	-0.651	0.000225	*1500012F01Rik*	-0.8327	0.000797	*Pdk1*	-1.328	4.88E-11
Pim1	-0.6511	0.005347	*Sdc4*	-0.8346	5.88E-07	*Epm2a*	-1.332	7.19E-07
Rnf217	-0.6521	0.000996	*Dusp10*	-0.8355	0.000648	*Gbe1*	-1.335	4.73E-08
Fosl1	-0.6555	0.002323	*Wisp2*	-0.8357	0.002311	*Fam162a*	-1.339	3.13E-12
Pde4d	-0.6574	0.003266	*Egln3*	-0.8368	0.00219	*Klk8*	-1.339	3.10E-07
Ankrd1	-0.6581	0.006869	*Kdm4b*	-0.8376	2.49E-05	*Tnfrsf9*	-1.354	1.14E-07
Acp6	-0.6599	0.000703	*Rbm3*	-0.8406	2.16E-05	*Dhrs3*	-1.356	2.19E-08
Pax9	-0.6611	0.007406	*Dusp4*	-0.8412	0.001316	*Il33*	-1.371	2.98E-08

Zc3h6	-0.664	0.012326	*Adam8*	-0.8434	3.58E-05	*Pgk1*	-1.373	1.29E-12
Chil3	-0.6642	0.009666	*Srgap3*	-0.8478	0.001996	*Ndrg1*	-1.379	1.82E-12
Plod2	-0.665	0.000192	*Inpp4b*	-0.8496	9.85E-05	*Cdkn1a*	-1.386	7.33E-12
Figf	-0.669	0.005873	*Btg2*	-0.8506	0.001491	*Mt2*	-1.387	4.26E-11
Crlf1	-0.6699	0.009754	*Herc3*	-0.8566	0.001592	*Per1*	-1.398	5.28E-10
Fam117b	-0.6727	0.000182	*2610528A11Rik*	-0.8567	0.001303	*Bnip3l*	-1.412	8.59E-12
Myo1h	-0.6729	0.01367	*Xdh*	-0.8626	0.000276	*Ccng2*	-1.46	4.84E-11
Foxg1	-0.6741	0.004553	*Rap2c*	-0.8653	0.000167	*Egln1*	-1.464	1.37E-16
Bsg	-0.6756	7.07E-05	*Zfp395*	-0.8679	0.000391	*Mt1*	-1.489	7.35E-16
Acap1	-0.6769	0.01348	*Itga10*	-0.8683	0.00136	*F3*	-1.492	1.65E-11
Appl2	-0.6775	0.001094	*Rcor2*	-0.8685	1.01E-06	*Prl2c2*	-1.504	2.66E-09
Csrnp1	-0.6779	0.002688	*Ctnnal1*	-0.8729	8.88E-05	*Hilpda*	-1.516	2.39E-13
Cav2	-0.6783	0.001056	*Abcg2*	-0.877	0.000658	*Slc2a1*	-1.543	4.68E-13
Gng2	-0.6783	0.009564	*Sema3f*	-0.8781	6.16E-05	*Selenbp1*	-1.567	3.43E-12
Lypd8	-0.6789	0.01081	*Dusp1*	-0.8789	0.001081	*Hmox1*	-1.6	2.72E-12
Trib1	-0.682	0.002135	*Fosl2*	-0.8864	1.29E-07	*Mpp2*	-1.601	2.32E-10
Pafah1b3	-0.6831	6.93E-05	*Trappc6a*	-0.8884	7.16E-05	*Ier3*	-1.644	1.07E-14
Btg1	-0.6847	0.000143	*Gm11110*	-0.8939	0.000429	*Ero1l*	-1.677	2.43E-15
Sdpr	-0.6855	0.003124	*Gpr35*	-0.8982	0.000933	*Ndufa4l2*	-1.813	2.81E-16
Adam22	-0.6862	0.01062	*Haghl*	-0.9003	0.000282	*Apln*	-1.841	4.22E-16
Serpinb9g	-0.6899	0.004293	*Dusp5*	-0.9142	0.000107	*Ankrd37*	-1.881	4.00E-15
Bnc1	-0.6903	0.007763	*Grhpr*	-0.9148	5.56E-08	*Nrn1*	-2.209	4.20E-18
Hoxb13	-0.6909	0.00556	*Pi15*	-0.9182	0.000224	*Bnip3*	-2.211	9.17E-25

Supplementary Figure 7. Predicted target genes for hsa-miR-29a-3p, overlapping with up- and down-regulated genes identified in sorted MC-38 cells in sorted HIF-KD tumor cells vs. sorted Mock cells. hsa-miR-29a-3p [1] target genes were identified using MicroRNA Data Integration Portal, mirDIP version 4.1.11.1 (Database version 4.1.0.3) (http://ophid.utoronto.ca/mirDIP) [2], using all 30 datasets, high confidence level, and bi-directional search option. While the table lists all known sources for individual genes, there are 81 unique up-regulated targets and 87 unique down-regulated targets.

Upregulated Gene targeted by mir29

	Gene Symbol	Uniprot	Source	Confidence class
UP	**ABCA13**	Q86UQ4	microrna.org	High
UP	**ADGRA3**	Q8IWK6	microrna.org	Very High
UP	**AKAP13**	Q12802	CoMeTa	High
UP	**AKAP13**	Q12802	ElMMo3	Very High
UP	**AKAP13**	Q12802	MultiMiTar	High
UP	**AKAP13**	Q12802	PACCMIT	High
UP	**AKAP13**	Q12802	TargetRank	Very High
UP	**AKAP13**	Q12802	TargetScan	Very High
UP	**AKAP13**	Q12802	miRTar2GO	High
UP	**AKAP13**	Q12802	MirAncesTar	High
UP	**AKAP13**	Q12802	microrna.org	High
UP	**AMOT**	Q4VCS5	CoMeTa	High
UP	**AMOT**	Q4VCS5	Cupid	High
UP	**AMOT**	Q4VCS5	ElMMo3	Very High
UP	**AMOT**	Q4VCS5	MAMI	High
UP	**AMOT**	Q4VCS5	MultiMiTar	High
UP	**AMOT**	Q4VCS5	PACCMIT	High
UP	**AMOT**	Q4VCS5	TargetRank	Very High
UP	**AMOT**	Q4VCS5	TargetScan	Very High
UP	**AMOT**	Q4VCS5	miRTar2GO	High
UP	**AMOT**	Q4VCS5	microrna.org	High
UP	**ANK1**	P16157	CoMeTa	High
UP	**ANK1**	P16157	Cupid	Very High
UP	**ANK1**	P16157	ElMMo3	Very High
UP	**ANK1**	P16157	PACCMIT	High
UP	**ANK1**	P16157	TargetScan	Very High
UP	**APC**	P25054	TargetScan	Very High
UP	**APC**	P25054	microrna.org	Very High
UP	**APOL6**	Q9BWW8	miRTar2GO	High
UP	**ARAP2**	Q8WZ64	microrna.org	High

UP	**ARAP3**	Q8WWN8	CoMeTa	High
UP	**ARAP3**	Q8WWN8	ElMMo3	High
UP	**ARAP3**	Q8WWN8	MAMI	High
UP	**ARAP3**	Q8WWN8	microrna.org	High
UP	**ATP2B4**	P23634	CoMeTa	Very High
UP	**ATP2B4**	P23634	Cupid	Very High
UP	**ATP2B4**	P23634	ElMMo3	Very High
UP	**ATP2B4**	P23634	MultiMiTar	High
UP	**ATP2B4**	P23634	PACCMIT	High
UP	**ATP2B4**	P23634	TargetRank	High
UP	**ATP2B4**	P23634	TargetScan	Very High
UP	**ATP2B4**	P23634	miRTar2GO	High
UP	**ATP2B4**	P23634	microrna.org	High
UP	**BCL2**	P10415	CoMeTa	High
UP	**BDP1**	A6H8Y1	miRTar2GO	High
UP	**BPTF**	Q12830	Cupid	Very High
UP	**BPTF**	Q12830	ElMMo3	High
UP	**CAMK2A**	Q9UQM7	MultiMiTar	High
UP	**CAMSAP1**	Q5T5Y3	miRTar2GO	High
UP	**CCDC36**	Q8IYA8	MAMI	High
UP	**CCDC36**	Q8IYA8	microrna.org	Very High
UP	**CCNE1**	P24864	Cupid	Very High
UP	**CCNE1**	P24864	ElMMo3	High
UP	**CCNE1**	P24864	miRTar2GO	High
UP	**CD276**	Q5ZPR3	ElMMo3	Very High
UP	**CD276**	Q5ZPR3	MAMI	High
UP	**CD276**	Q5ZPR3	PACCMIT	High
UP	**CD276**	Q5ZPR3	TargetRank	Very High
UP	**CD276**	Q5ZPR3	TargetScan	Very High
UP	**CD276**	Q5ZPR3	miRTar2GO	High
UP	**CD276**	Q5ZPR3	microrna.org	High
UP	**COL1A1**	P02452	CoMeTa	High
UP	**COL1A1**	P02452	Cupid	Very High
UP	**COL1A1**	P02452	DIANA	High
UP	**COL1A1**	P02452	ElMMo3	Very High
UP	**COL1A1**	P02452	GenMir++	Very High
UP	**COL1A1**	P02452	MAMI	Very High
UP	**COL1A1**	P02452	Mirza-G	High
UP	**COL1A1**	P02452	MultiMiTar	High
UP	**COL1A1**	P02452	PACCMIT	High
UP	**COL1A1**	P02452	TargetRank	High
UP	**COL1A1**	P02452	TargetScan	Very High
UP	**COL1A1**	P02452	miRTar2GO	High
UP	**COL1A1**	P02452	microrna.org	High
UP	**COL27A1**	Q8IZC6	DIANA	High
UP	**COL27A1**	Q8IZC6	PACCMIT	High

UP	**COL27A1**	Q8IZC6	TargetScan	Very High
UP	**COL2A1**	P02458	CoMeTa	High
UP	**COL2A1**	P02458	DIANA	Very High
UP	**COL2A1**	P02458	ElMMo3	Very High
UP	**COL2A1**	P02458	MirTar	High
UP	**COL2A1**	P02458	PicTar	Very High
UP	**COL2A1**	P02458	TargetRank	Very High
UP	**COL2A1**	P02458	TargetScan	Very High
UP	**COL2A1**	P02458	miRDB	High
UP	**COL2A1**	P02458	microrna.org	Very High
UP	**COL3A1**	P02461	CoMeTa	Very High
UP	**COL3A1**	P02461	Cupid	Very High
UP	**COL3A1**	P02461	DIANA	Very High
UP	**COL3A1**	P02461	ElMMo3	Very High
UP	**COL3A1**	P02461	MAMI	Very High
UP	**COL3A1**	P02461	MirTar	Very High
UP	**COL3A1**	P02461	Mirza-G	High
UP	**COL3A1**	P02461	MultiMiTar	High
UP	**COL3A1**	P02461	PACCMIT	High
UP	**COL3A1**	P02461	PicTar	Very High
UP	**COL3A1**	P02461	TargetRank	Very High
UP	**COL3A1**	P02461	TargetScan	Very High
UP	**COL3A1**	P02461	miRDB	High
UP	**COL3A1**	P02461	microrna.org	Very High
UP	**COL5A2**	P05997	CoMeTa	Very High
UP	**COL5A2**	P05997	Cupid	Very High
UP	**COL5A2**	P05997	DIANA	High
UP	**COL5A2**	P05997	ElMMo3	Very High
UP	**COL5A2**	P05997	MirTar	High
UP	**COL5A2**	P05997	Mirza-G	High
UP	**COL5A2**	P05997	PACCMIT	High
UP	**COL5A2**	P05997	PicTar	Very High
UP	**COL5A2**	P05997	TargetScan	Very High
UP	**COL5A2**	P05997	miRDB	High
UP	**COL5A2**	P05997	miRTar2GO	High
UP	**COL5A2**	P05997	microrna.org	Very High
UP	**CSPG4**	Q6UVK1	ElMMo3	High
UP	**CSPG4**	Q6UVK1	MAMI	High
UP	**CSPG4**	Q6UVK1	PACCMIT	High
UP	**CSPG4**	Q6UVK1	TargetScan	Very High
UP	**CSPG4**	Q6UVK1	microrna.org	High
UP	**DENND3**	A2RUS2	microrna.org	High
UP	**EML5**	Q05BV3	Cupid	Very High
UP	**EML5**	Q05BV3	DIANA	High
UP	**EML5**	Q05BV3	ElMMo3	Very High
UP	**EML5**	Q05BV3	MAMI	High

UP	**EML5**	Q05BV3	PACCMIT	High
UP	**EML5**	Q05BV3	TargetScan	Very High
UP	**EML5**	Q05BV3	miRDB	High
UP	**EML5**	Q05BV3	miRTar2GO	High
UP	**EML5**	Q05BV3	microrna.org	High
UP	**ENPP2**	Q13822	CoMeTa	High
UP	**ENPP2**	Q13822	Cupid	Very High
UP	**ENPP2**	Q13822	TargetRank	Very High
UP	**ENPP2**	Q13822	TargetScan	Very High
UP	**ENPP2**	Q13822	microrna.org	Very High
UP	**FAS**	P25445	CoMeTa	High
UP	**FAS**	P25445	microrna.org	High
UP	**GLI2**	P10070	miRTar2GO	High
UP	**GLI2**	P10070	microrna.org	High
UP	**GOLGA3**	Q08378	miRTar2GO	High
UP	**GRIP1**	Q9Y3R0	DIANA	Very High
UP	**GRIP1**	Q9Y3R0	ElMMo3	Very High
UP	**GRIP1**	Q9Y3R0	MAMI	High
UP	**GRIP1**	Q9Y3R0	TargetScan	Very High
UP	**GRIP1**	Q9Y3R0	miRTar2GO	High
UP	**GRIP1**	Q9Y3R0	microrna.org	Very High
UP	**GXYLT2**	A0PJZ3	Cupid	Very High
UP	**GXYLT2**	A0PJZ3	DIANA	High
UP	**GXYLT2**	A0PJZ3	ElMMo3	Very High
UP	**GXYLT2**	A0PJZ3	TargetScan	Very High
UP	**GXYLT2**	A0PJZ3	miRTar2GO	High
UP	**GXYLT2**	A0PJZ3	microrna.org	Very High
UP	**HAS2**	Q92819	TargetScan	Very High
UP	**HIP1**	O00291	CoMeTa	High
UP	**HIP1**	O00291	ElMMo3	High
UP	**HIP1**	O00291	TargetScan	Very High
UP	**HIP1**	O00291	MirAncesTar	High
UP	**KIF26B**	Q2KJY2	CoMeTa	High
UP	**KIF26B**	Q2KJY2	Cupid	Very High
UP	**KIF26B**	Q2KJY2	DIANA	Very High
UP	**KIF26B**	Q2KJY2	ElMMo3	Very High
UP	**KIF26B**	Q2KJY2	MAMI	High
UP	**KIF26B**	Q2KJY2	PACCMIT	High
UP	**KIF26B**	Q2KJY2	TargetRank	Very High
UP	**KIF26B**	Q2KJY2	TargetScan	Very High
UP	**KIF26B**	Q2KJY2	miRDB	High
UP	**KIF26B**	Q2KJY2	microrna.org	Very High
UP	**LAMC1**	P11047	CoMeTa	Very High
UP	**LAMC1**	P11047	DIANA	High
UP	**LAMC1**	P11047	ElMMo3	Very High
UP	**LAMC1**	P11047	MAMI	Very High

UP	**LAMC1**	P11047	Mirza-G	High
UP	**LAMC1**	P11047	PACCMIT	High
UP	**LAMC1**	P11047	TargetRank	Very High
UP	**LAMC1**	P11047	TargetScan	Very High
UP	**LAMC1**	P11047	miRDB	High
UP	**LAMC1**	P11047	MirAncesTar	High
UP	**LAMC1**	P11047	microrna.org	Very High
UP	**LBP**	P18428	CoMeTa	High
UP	**MAGI1**	Q96QZ7	CoMeTa	High
UP	**MDN1**	Q9NU22	miRTar2GO	High
UP	**MMP28**	Q9H239	microrna.org	High
UP	**MYO18A**	Q92614	ElMMo3	High
UP	**MYO18A**	Q92614	MultiMiTar	High
UP	**MYO18A**	Q92614	PACCMIT	High
UP	**MYO18A**	Q92614	TargetScan	Very High
UP	**NAV1**	Q8NEY1	CoMeTa	High
UP	**NAV1**	Q8NEY1	Cupid	Very High
UP	**NAV1**	Q8NEY1	DIANA	High
UP	**NAV1**	Q8NEY1	ElMMo3	Very High
UP	**NAV1**	Q8NEY1	MirTar	High
UP	**NAV1**	Q8NEY1	Mirza-G	High
UP	**NAV1**	Q8NEY1	MultiMiTar	High
UP	**NAV1**	Q8NEY1	PACCMIT	High
UP	**NAV1**	Q8NEY1	TargetRank	High
UP	**NAV1**	Q8NEY1	TargetScan	Very High
UP	**NAV1**	Q8NEY1	miRTar2GO	High
UP	**NAV1**	Q8NEY1	microrna.org	High
UP	**NCAM1**	P13591	CoMeTa	High
UP	**NCAM1**	P13591	microrna.org	High
UP	**NCKAP5**	O14513	Cupid	Very High
UP	**NCKAP5**	O14513	ElMMo3	Very High
UP	**NCKAP5**	O14513	MAMI	High
UP	**NCKAP5**	O14513	Mirza-G	High
UP	**NCKAP5**	O14513	PACCMIT	High
UP	**NCKAP5**	O14513	TargetRank	Very High
UP	**NCKAP5**	O14513	TargetScan	Very High
UP	**NCKAP5**	O14513	miRDB	High
UP	**NCKAP5**	O14513	microrna.org	Very High
UP	**NID2**	Q14112	CoMeTa	High
UP	**NID2**	Q14112	Cupid	Very High
UP	**NID2**	Q14112	ElMMo3	Very High
UP	**NID2**	Q14112	MAMI	High
UP	**NID2**	Q14112	microrna.org	High
UP	**NIN**	Q8N4C6	miRTar2GO	High
UP	**NIPBL**	Q6KC79	microrna.org	High
UP	**NOL4L**	Q96MY1	Cupid	Very High

UP	**NOL4L**	Q96MY1	ElMMo3	Very High
UP	**NOL4L**	Q96MY1	Mirza-G	High
UP	**NOL4L**	Q96MY1	TargetScan	Very High
UP	**NOL4L**	Q96MY1	miRTar2GO	High
UP	**NOL4L**	Q96MY1	MirAncesTar	High
UP	**NOL4L**	Q96MY1	microrna.org	High
UP	**PCSK9**	Q8NBP7	miRTar2GO	High
UP	**PDGFA**	P04085	MultiMiTar	High
UP	**PENK**	P01210	MAMI	High
UP	**PLXNA1**	Q9UIW2	CoMeTa	High
UP	**PLXNA1**	Q9UIW2	ElMMo3	High
UP	**PLXNA1**	Q9UIW2	MultiMiTar	High
UP	**PLXNA1**	Q9UIW2	PicTar	Very High
UP	**PLXNA1**	Q9UIW2	TargetRank	Very High
UP	**PLXNA1**	Q9UIW2	TargetScan	Very High
UP	**PLXNA1**	Q9UIW2	miRDB	High
UP	**PLXNA1**	Q9UIW2	miRTar2GO	High
UP	**PLXNA1**	Q9UIW2	microrna.org	High
UP	**RABL6**	Q3YEC7	miRTar2GO	High
UP	**RABL6**	Q3YEC7	microrna.org	High
UP	**SCML4**	Q8N228	microrna.org	High
UP	**SEMA3C**	Q99985	miRTar2GO	High
UP	**SEMA6A**	Q9H2E6	microrna.org	High
UP	**SERPINH1**	P50454	CoMeTa	Very High
UP	**SERPINH1**	P50454	Cupid	Very High
UP	**SERPINH1**	P50454	DIANA	High
UP	**SERPINH1**	P50454	ElMMo3	Very High
UP	**SERPINH1**	P50454	MultiMiTar	High
UP	**SERPINH1**	P50454	TargetScan	Very High
UP	**SERTAD4**	Q9NUC0	MirTar	High
UP	**SERTAD4**	Q9NUC0	TargetRank	High
UP	**SERTAD4**	Q9NUC0	microrna.org	High
UP	**SH3PXD2A**	Q5TCZ1	CoMeTa	High
UP	**SH3PXD2A**	Q5TCZ1	Cupid	Very High
UP	**SH3PXD2A**	Q5TCZ1	DIANA	Very High
UP	**SH3PXD2A**	Q5TCZ1	ElMMo3	Very High
UP	**SH3PXD2A**	Q5TCZ1	Mirza-G	High
UP	**SH3PXD2A**	Q5TCZ1	PACCMIT	Very High
UP	**SH3PXD2A**	Q5TCZ1	TargetRank	High
UP	**SH3PXD2A**	Q5TCZ1	TargetScan	Very High
UP	**SH3PXD2A**	Q5TCZ1	miRTar2GO	High
UP	**SLC2A13**	Q96QE2	MultiMiTar	High
UP	**SLITRK5**	O94991	Cupid	Very High
UP	**SPRY1**	O43609	CoMeTa	High
UP	**SPRY1**	O43609	Cupid	Very High
UP	**SPRY1**	O43609	ElMMo3	Very High

UP	**SPRY1**	O43609	Mirza-G	High
UP	**SPRY1**	O43609	PACCMIT	High
UP	**SPRY1**	O43609	TargetScan	Very High
UP	**SPRY1**	O43609	microrna.org	Very High
UP	**SSH2**	Q76I76	ElMMo3	High
UP	**SSH2**	Q76I76	MultiMiTar	High
UP	**SSH2**	Q76I76	PACCMIT	High
UP	**SSH2**	Q76I76	miRTar2GO	High
UP	**STMN2**	Q93045	DIANA	Very High
UP	**STMN2**	Q93045	ElMMo3	Very High
UP	**STMN2**	Q93045	PACCMIT	High
UP	**STMN2**	Q93045	TargetScan	Very High
UP	**SYNE2**	Q8WXH0	CoMeTa	High
UP	**SYNE2**	Q8WXH0	microrna.org	High
UP	**SYNJ2**	O15056	microrna.org	High
UP	**TENM3**	Q9P273	CoMeTa	High
UP	**TENM3**	Q9P273	Cupid	High
UP	**TENM3**	Q9P273	ElMMo3	Very High
UP	**TENM3**	Q9P273	TargetScan	Very High
UP	**TENM3**	Q9P273	microrna.org	High
UP	**THBS2**	P35442	TargetRank	Very High
UP	**THBS2**	P35442	microrna.org	Very High
UP	**TMEM159**	Q96B96	microrna.org	High
UP	**TNRC6C**	Q9HCJ0	microrna.org	High
UP	**TRAK2**	O60296	ElMMo3	High
UP	**TRAK2**	O60296	MultiMiTar	High
UP	**TRAK2**	O60296	PACCMIT	High
UP	**TRAK2**	O60296	TargetScan	Very High
UP	**TRAK2**	O60296	miRTar2GO	High
UP	**TRAK2**	O60296	microrna.org	High
UP	**TRIM56**	Q9BRZ2	microrna.org	High
UP	**UHRF1BP1**	Q6BDS2	ElMMo3	High
UP	**UHRF1BP1**	Q6BDS2	MultiMiTar	High
UP	**UHRF1BP1**	Q6BDS2	miRTar2GO	High
UP	**UHRF1BP1**	Q6BDS2	microrna.org	High
UP	**UNC5B**	Q8IZJ1	microrna.org	High
UP	**URB1**	O60287	TargetScan	Very High
UP	**WDFY3**	Q8IZQ1	CoMeTa	Very High
UP	**WDFY3**	Q8IZQ1	Cupid	Very High
UP	**WDFY3**	Q8IZQ1	ElMMo3	Very High
UP	**WDFY3**	Q8IZQ1	MultiMiTar	High
UP	**WDFY3**	Q8IZQ1	PACCMIT	High
UP	**WDFY3**	Q8IZQ1	TargetScan	Very High
UP	**WDFY3**	Q8IZQ1	miRTar2GO	High
UP	**WISP1**	O95388	TargetScan	Very High
UP	**WISP1**	O95388	MirAncesTar	High

UP	**WISP1**	O95388	microrna.org	High
UP	**XYLT1**	Q86Y38	MultiMiTar	High
UP	**ZBTB40**	Q9NUA8	CoMeTa	High
UP	**ZBTB40**	Q9NUA8	Cupid	Very High
UP	**ZBTB40**	Q9NUA8	ElMMo3	Very High
UP	**ZBTB40**	Q9NUA8	MAMI	High
UP	**ZBTB40**	Q9NUA8	MultiMiTar	High
UP	**ZBTB40**	Q9NUA8	PACCMIT	High
UP	**ZBTB40**	Q9NUA8	TargetScan	Very High
UP	**ZBTB40**	Q9NUA8	MirAncesTar	High
UP	**ZBTB40**	Q9NUA8	microrna.org	High
UP	**ZNF251**	Q9BRH9	microrna.org	High
UP	**ZNF616**	Q08AN1	microrna.org	High

Downregulated Gene targeted by mir29

	Gene Symbol	Uniprot	Source	Confidence class
DOWN	**ABHD18**	Q0P651	TargetScan	Very High
DOWN	**ADAM22**	Q9P0K1	ElMMo3	Very High
DOWN	**ADAM8**	P78325	microrna.org	High
DOWN	**AK4**	P27144	CoMeTa	High
DOWN	**AK4**	P27144	ElMMo3	High
DOWN	**AK4**	P27144	microrna.org	High
DOWN	**AMPD3**	Q01432	MultiMiTar	High
DOWN	**AMPD3**	Q01432	microrna.org	High
DOWN	**ANGPTL4**	Q9BY76	CoMeTa	High
DOWN	**ANGPTL4**	Q9BY76	ElMMo3	High
DOWN	**ANGPTL4**	Q9BY76	MAMI	Very High
DOWN	**ANGPTL4**	Q9BY76	microrna.org	High
DOWN	**ARRDC3**	Q96B67	Cupid	Very High
DOWN	**ARRDC3**	Q96B67	DIANA	High
DOWN	**ARRDC3**	Q96B67	ElMMo3	Very High
DOWN	**ARRDC3**	Q96B67	MirTar	High
DOWN	**ARRDC3**	Q96B67	Mirza-G	High
DOWN	**ARRDC3**	Q96B67	MultiMiTar	High
DOWN	**ARRDC3**	Q96B67	PACCMIT	High
DOWN	**ARRDC3**	Q96B67	TargetRank	High
DOWN	**ARRDC3**	Q96B67	TargetScan	Very High
DOWN	**ARRDC3**	Q96B67	miRDB	High
DOWN	**ARRDC3**	Q96B67	miRTar2GO	High
DOWN	**ARRDC3**	Q96B67	MirAncesTar	High
DOWN	**ARRDC3**	Q96B67	microrna.org	Very High
DOWN	**BMT2**	Q1RMZ1	Cupid	Very High
DOWN	**BMT2**	Q1RMZ1	DIANA	High

DOWN	**BMT2**	Q1RMZ1	EIMMo3	Very High
DOWN	**BMT2**	Q1RMZ1	Mirza-G	High
DOWN	**BMT2**	Q1RMZ1	PACCMIT	High
DOWN	**BMT2**	Q1RMZ1	TargetRank	High
DOWN	**BMT2**	Q1RMZ1	TargetScan	Very High
DOWN	**BMT2**	Q1RMZ1	miRDB	High
DOWN	**BMT2**	Q1RMZ1	miRTar2GO	High
DOWN	**BMT2**	Q1RMZ1	microrna.org	Very High
DOWN	**BSG**	P35613	microrna.org	High
DOWN	**BTG1**	P62324	microrna.org	Very High
DOWN	**BTG2**	P78543	CoMeTa	High
DOWN	**BTG2**	P78543	Cupid	Very High
DOWN	**BTG2**	P78543	DIANA	High
DOWN	**BTG2**	P78543	EIMMo3	Very High
DOWN	**BTG2**	P78543	MultiMiTar	High
DOWN	**BTG2**	P78543	PACCMIT	High
DOWN	**BTG2**	P78543	TargetScan	Very High
DOWN	**BTG2**	P78543	miRTar2GO	High
DOWN	**CAV2**	P51636	CoMeTa	Very High
DOWN	**CAV2**	P51636	Cupid	Very High
DOWN	**CAV2**	P51636	DIANA	High
DOWN	**CAV2**	P51636	EIMMo3	Very High
DOWN	**CAV2**	P51636	MAMI	Very High
DOWN	**CAV2**	P51636	Mirza-G	High
DOWN	**CAV2**	P51636	PACCMIT	High
DOWN	**CAV2**	P51636	TargetScan	Very High
DOWN	**CAV2**	P51636	miRDB	High
DOWN	**CAV2**	P51636	miRTar2GO	High
DOWN	**CAV2**	P51636	microrna.org	Very High
DOWN	**CD109**	Q6YHK3	miRTar2GO	High
DOWN	**CDKN1A**	P38936	miRTar2GO	High
DOWN	**CDKN2D**	P55273	miRTar2GO	High
DOWN	**CELF2**	O95319	CoMeTa	Very High
DOWN	**CELF2**	O95319	Cupid	Very High
DOWN	**CELF2**	O95319	EIMMo3	Very High
DOWN	**CELF2**	O95319	Mirza-G	High
DOWN	**CELF2**	O95319	MultiMiTar	High
DOWN	**CELF2**	O95319	PACCMIT	High
DOWN	**CELF2**	O95319	TargetRank	Very High
DOWN	**CELF2**	O95319	TargetScan	Very High
DOWN	**CELF2**	O95319	miRTar2GO	High
DOWN	**CELF2**	O95319	microrna.org	Very High
DOWN	**CIRBP**	Q14011	microrna.org	High
DOWN	**CNR1**	P21554	CoMeTa	High
DOWN	**CNR1**	P21554	Cupid	Very High
DOWN	**CNR1**	P21554	EIMMo3	Very High

DOWN	**CNR1**	P21554	MultiMiTar	High
DOWN	**CNR1**	P21554	PACCMIT	High
DOWN	**CNR1**	P21554	TargetRank	Very High
DOWN	**CNR1**	P21554	TargetScan	Very High
DOWN	**CNR1**	P21554	MirAncesTar	High
DOWN	**CNR1**	P21554	microrna.org	High
DOWN	**CYR61**	O00622	miRTar2GO	High
DOWN	**DMXL1**	Q9Y485	MultiMiTar	High
DOWN	**DMXL1**	Q9Y485	microrna.org	High
DOWN	**DNAJC5**	Q9H3Z4	miRTar2GO	High
DOWN	**DUSP4**	Q13115	miRTar2GO	High
DOWN	**EPHA7**	Q15375	microrna.org	High
DOWN	**EPS8L2**	Q9H6S3	MAMI	High
DOWN	**FAM117B**	Q6P1L5	miRTar2GO	High
DOWN	**FAM117B**	Q6P1L5	microrna.org	High
DOWN	**FAM46B**	Q96A09	MAMI	High
DOWN	**FGF7**	P21781	microrna.org	Very High
DOWN	**FRAT2**	O75474	CoMeTa	High
DOWN	**FRAT2**	O75474	Cupid	Very High
DOWN	**FRAT2**	O75474	ElMMo3	Very High
DOWN	**FRAT2**	O75474	PACCMIT	High
DOWN	**FRAT2**	O75474	TargetRank	Very High
DOWN	**FRAT2**	O75474	TargetScan	Very High
DOWN	**FRAT2**	O75474	miRTar2GO	High
DOWN	**FRAT2**	O75474	MirAncesTar	High
DOWN	**FRAT2**	O75474	microrna.org	Very High
DOWN	**GNG2**	P59768	Cupid	Very High
DOWN	**GNG2**	P59768	ElMMo3	High
DOWN	**GNG2**	P59768	PACCMIT	High
DOWN	**GNG2**	P59768	TargetScan	Very High
DOWN	**GNG2**	P59768	microrna.org	High
DOWN	**GPI**	P06744	MirTar	High
DOWN	**GPI**	P06744	miRTar2GO	High
DOWN	**GPI**	P06744	microrna.org	High
DOWN	**GRIA4**	P48058	MultiMiTar	High
DOWN	**GRIA4**	P48058	microrna.org	High
DOWN	**GYS1**	P13807	microrna.org	High
DOWN	**HBEGF**	Q99075	CoMeTa	High
DOWN	**HBEGF**	Q99075	Cupid	Very High
DOWN	**HBEGF**	Q99075	DIANA	High
DOWN	**HBEGF**	Q99075	ElMMo3	Very High
DOWN	**HBEGF**	Q99075	MultiMiTar	High
DOWN	**HBEGF**	Q99075	TargetScan	Very High
DOWN	**HBEGF**	Q99075	miRTar2GO	High
DOWN	**HBEGF**	Q99075	microrna.org	High
DOWN	**HBP1**	O60381	CoMeTa	Very High

DOWN	**HBP1**	O60381	Cupid	Very High
DOWN	**HBP1**	O60381	DIANA	Very High
DOWN	**HBP1**	O60381	EIMMo3	Very High
DOWN	**HBP1**	O60381	MAMI	Very High
DOWN	**HBP1**	O60381	MirTar	High
DOWN	**HBP1**	O60381	Mirza-G	High
DOWN	**HBP1**	O60381	MultiMiTar	High
DOWN	**HBP1**	O60381	PACCMIT	High
DOWN	**HBP1**	O60381	TargetRank	Very High
DOWN	**HBP1**	O60381	TargetScan	Very High
DOWN	**HBP1**	O60381	miRDB	High
DOWN	**HBP1**	O60381	microrna.org	Very High
DOWN	**HERC3**	Q15034	microrna.org	High
DOWN	**HIGD1A**	Q9Y241	miRTar2GO	High
DOWN	**HLF**	Q16534	CoMeTa	High
DOWN	**HLF**	Q16534	EIMMo3	Very High
DOWN	**HLF**	Q16534	TargetRank	Very High
DOWN	**HLF**	Q16534	TargetScan	Very High
DOWN	**HLF**	Q16534	microrna.org	High
DOWN	**HOGA1**	Q86XE5	microrna.org	High
DOWN	**HOMER1**	Q86YM7	TargetScan	Very High
DOWN	**ID3**	Q02535	MultiMiTar	High
DOWN	**ID3**	Q02535	miRTar2GO	High
DOWN	**ID3**	Q02535	microrna.org	High
DOWN	**IER2**	Q9BTL4	miRTar2GO	High
DOWN	**ISLR2**	Q6UXK2	Cupid	Very High
DOWN	**ISLR2**	Q6UXK2	DIANA	High
DOWN	**ISLR2**	Q6UXK2	EIMMo3	Very High
DOWN	**ISLR2**	Q6UXK2	PACCMIT	High
DOWN	**ISLR2**	Q6UXK2	TargetScan	Very High
DOWN	**ISLR2**	Q6UXK2	MirAncesTar	High
DOWN	**ISLR2**	Q6UXK2	microrna.org	High
DOWN	**JUN**	P05412	microrna.org	High
DOWN	**KDM4B**	O94953	CoMeTa	High
DOWN	**KDM4B**	O94953	Cupid	Very High
DOWN	**KDM4B**	O94953	EIMMo3	High
DOWN	**KDM4B**	O94953	TargetScan	Very High
DOWN	**KLF11**	O14901	CoMeTa	High
DOWN	**KLF11**	O14901	miRTar2GO	High
DOWN	**KLF11**	O14901	microrna.org	Very High
DOWN	**KLF2**	Q9Y5W3	microrna.org	High
DOWN	**KLHL24**	Q6TFL4	EIMMo3	High
DOWN	**KLHL24**	Q6TFL4	MultiMiTar	High
DOWN	**LOX**	P28300	Cupid	Very High
DOWN	**LOX**	P28300	DIANA	High
DOWN	**LOX**	P28300	EIMMo3	Very High

DOWN	**LOX**	P28300	MirTar	High
DOWN	**LOX**	P28300	Mirza-G	High
DOWN	**LOX**	P28300	TargetScan	Very High
DOWN	**LOX**	P28300	miRDB	High
DOWN	**LOX**	P28300	miRTar2GO	High
DOWN	**LOX**	P28300	MirAncesTar	High
DOWN	**LOX**	P28300	microrna.org	High
DOWN	**MCTP2**	Q6DN12	microrna.org	High
DOWN	**MPP2**	Q14168	MultiMiTar	High
DOWN	**MXI1**	P50539	CoMeTa	Very High
DOWN	**MXI1**	P50539	Cupid	Very High
DOWN	**MXI1**	P50539	ElMMo3	Very High
DOWN	**MXI1**	P50539	TargetScan	Very High
DOWN	**MYO1H**	Q8N1T3	microrna.org	High
DOWN	**NAMPT**	P43490	microrna.org	Very High
DOWN	**NSUN3**	Q9H649	CoMeTa	High
DOWN	**OTUD1**	Q5VV17	Cupid	Very High
DOWN	**OTUD1**	Q5VV17	ElMMo3	High
DOWN	**OTUD1**	Q5VV17	microrna.org	High
DOWN	**PCGF5**	Q86SE9	MultiMiTar	High
DOWN	**PCGF5**	Q86SE9	miRTar2GO	High
DOWN	**PDK1**	Q15118	miRTar2GO	High
DOWN	**PDK1**	Q15118	microrna.org	High
DOWN	**PER1**	O15534	CoMeTa	High
DOWN	**PER1**	O15534	Cupid	Very High
DOWN	**PER1**	O15534	ElMMo3	Very High
DOWN	**PER1**	O15534	MAMI	High
DOWN	**PER1**	O15534	MultiMiTar	High
DOWN	**PER1**	O15534	PACCMIT	High
DOWN	**PER1**	O15534	TargetScan	Very High
DOWN	**PFKL**	P17858	miRTar2GO	High
DOWN	**PFKP**	Q01813	microrna.org	High
DOWN	**PI15**	O43692	CoMeTa	High
DOWN	**PI15**	O43692	Cupid	Very High
DOWN	**PI15**	O43692	DIANA	High
DOWN	**PI15**	O43692	ElMMo3	Very High
DOWN	**PI15**	O43692	MirTar	High
DOWN	**PI15**	O43692	Mirza-G	High
DOWN	**PI15**	O43692	MultiMiTar	High
DOWN	**PI15**	O43692	PACCMIT	Very High
DOWN	**PI15**	O43692	TargetRank	Very High
DOWN	**PI15**	O43692	TargetScan	Very High
DOWN	**PI15**	O43692	miRTar2GO	High
DOWN	**PI15**	O43692	MirAncesTar	High
DOWN	**PI15**	O43692	microrna.org	High
DOWN	**PIK3CB**	P42338	TargetScan	Very High

DOWN	**PNRC1**	Q12796	microrna.org	Very High
DOWN	**PRDM1**	O75626	CoMeTa	High
DOWN	**PRDM1**	O75626	Cupid	Very High
DOWN	**PRDM1**	O75626	ElMMo3	High
DOWN	**PRDM1**	O75626	miRTar2GO	High
DOWN	**PRDM1**	O75626	MirAncesTar	High
DOWN	**PRDM1**	O75626	microrna.org	High
DOWN	**PRKAB2**	O43741	CoMeTa	High
DOWN	**PRKAB2**	O43741	Cupid	Very High
DOWN	**PRKAB2**	O43741	DIANA	High
DOWN	**PRKAB2**	O43741	ElMMo3	Very High
DOWN	**PRKAB2**	O43741	MirTar	High
DOWN	**PRKAB2**	O43741	MultiMiTar	High
DOWN	**PRKAB2**	O43741	TargetRank	High
DOWN	**PRKAB2**	O43741	TargetScan	Very High
DOWN	**PRKAB2**	O43741	microrna.org	High
DOWN	**PTTG1IP**	P53801	miRTar2GO	High
DOWN	**PXMP4**	Q9Y6I8	CoMeTa	High
DOWN	**PXMP4**	Q9Y6I8	ElMMo3	High
DOWN	**PXMP4**	Q9Y6I8	MultiMiTar	High
DOWN	**PXMP4**	Q9Y6I8	TargetScan	Very High
DOWN	**PXMP4**	Q9Y6I8	MirAncesTar	High
DOWN	**RAP2C**	Q9Y3L5	microrna.org	Very High
DOWN	**RHOB**	P62745	CoMeTa	Very High
DOWN	**RNF217**	Q8TC41	TargetScan	Very High
DOWN	**RPS10**	P46783	MAMI	High
DOWN	**RPS24**	P62847	CoMeTa	High
DOWN	**RPS24**	P62847	miRTar2GO	High
DOWN	**RUSC2**	Q8N2Y8	miRTar2GO	High
DOWN	**SGK1**	O00141	CoMeTa	High
DOWN	**SGK1**	O00141	Cupid	Very High
DOWN	**SGK1**	O00141	ElMMo3	Very High
DOWN	**SGK1**	O00141	MAMI	High
DOWN	**SGK1**	O00141	MirTar	High
DOWN	**SGK1**	O00141	Mirza-G	High
DOWN	**SGK1**	O00141	MultiMiTar	High
DOWN	**SGK1**	O00141	PACCMIT	High
DOWN	**SGK1**	O00141	TargetScan	Very High
DOWN	**SGK1**	O00141	miRDB	High
DOWN	**SGK1**	O00141	miRTar2GO	High
DOWN	**SGK1**	O00141	MirAncesTar	High
DOWN	**SGK1**	O00141	microrna.org	Very High
DOWN	**SLC2A1**	P11166	CoMeTa	Very High
DOWN	**SRGAP3**	O43295	CoMeTa	High
DOWN	**SRGAP3**	O43295	MultiMiTar	High
DOWN	**SRGAP3**	O43295	MirAncesTar	High

DOWN	**TIPARP**	Q7Z3E1	CoMeTa	Very High
DOWN	**TNFRSF9**	Q07011	CoMeTa	High
DOWN	**TNFRSF9**	Q07011	Cupid	Very High
DOWN	**TNFRSF9**	Q07011	DIANA	High
DOWN	**TNFRSF9**	Q07011	MAMI	High
DOWN	**TNFRSF9**	Q07011	TargetRank	Very High
DOWN	**TNFRSF9**	Q07011	microrna.org	Very High
DOWN	**TPT1**	P13693	microrna.org	Very High
DOWN	**TXNIP**	Q9H3M7	miRTar2GO	High
DOWN	**UPK1B**	O75841	CoMeTa	High
DOWN	**UPK1B**	O75841	ElMMo3	High
DOWN	**UPK1B**	O75841	MAMI	High
DOWN	**UPK1B**	O75841	MultiMiTar	High
DOWN	**UPK1B**	O75841	PACCMIT	High
DOWN	**UPK1B**	O75841	TargetScan	Very High
DOWN	**UPK1B**	O75841	microrna.org	High
DOWN	**VIM**	P08670	CoMeTa	Very High
DOWN	**WISP2**	O76076	miRTar2GO	High
DOWN	**WWC1**	Q8IX03	MAMI	High
DOWN	**XDH**	P47989	ElMMo3	High
DOWN	**XDH**	P47989	TargetRank	Very High
DOWN	**XDH**	P47989	microrna.org	High
DOWN	**ZC3H6**	P61129	MultiMiTar	High
DOWN	**ZFP36**	P26651	CoMeTa	High
DOWN	**ZFP36**	P26651	Cupid	Very High
DOWN	**ZFP36**	P26651	ElMMo3	Very High
DOWN	**ZFP36**	P26651	MAMI	High
DOWN	**ZFP36**	P26651	TargetScan	Very High
DOWN	**ZFP36**	P26651	microrna.org	High

References:

[1] Rosano S, Cora D, Parab S, Zaffuto S, Isella C, Porporato R, Hoza RM, Calogero RA, Riganti C, Bussolino F, et al. (2020). A regulatory microRNA network controls endothelial cell phenotypic switch during sprouting angiogenesis *Elife* **9**.

[2] Tokar T, Pastrello C, Rossos AEM, Abovsky M, Hauschild AC, Tsay M, Lu R, Jurisica I (2018). mirDIP 4.1-integrative database of human microRNA target predictions *Nucleic Acids Res* **46**, D360-D370.